Original article

MOLECULAR METABOLISM

# Cardiomyocyte-specific deficiency of ketone body metabolism promotes accelerated pathological remodeling

**Rebecca C. Schugar [1], Ashley R. Moll [1], D. André d'Avignon [2], Carla J. Weinheimer [1], Attila Kovacs [1], Peter A. Crawford [1,3,*]**

## ABSTRACT

**Objective:** Exploitation of protective metabolic pathways within injured myocardium still remains an unclarified therapeutic target in heart disease. Moreover, while the roles of altered fatty acid and glucose metabolism in the failing heart have been explored, the influence of highly dynamic and nutritionally modifiable ketone body metabolism in the regulation of myocardial substrate utilization, mitochondrial bioenergetics, reactive oxygen species (ROS) generation, and hemodynamic response to injury remains undefined.

**Methods:** Here we use mice that lack the enzyme required for terminal oxidation of ketone bodies, succinyl-CoA:3-oxoacid CoA transferase (SCOT) to determine the role of ketone body oxidation in the myocardial injury response. Tracer delivery in *ex vivo* perfused hearts coupled to NMR spectroscopy, *in vivo* high-resolution echocardiographic quantification of cardiac hemodynamics in nutritionally and surgically modified mice, and cellular and molecular measurements of energetic and oxidative stress responses are performed.

**Results:** While germline SCOT-knockout (KO) mice die in the early postnatal period, adult mice with cardiomyocyte-specific loss of SCOT (SCOT-Heart-KO) remarkably exhibit no overt metabolic abnormalities, and no differences in left ventricular mass or impairments of systolic function during periods of ketosis, including fasting and adherence to a ketogenic diet. Myocardial fatty acid oxidation is increased when ketones are delivered but cannot be oxidized. To determine the role of ketone body oxidation in the remodeling ventricle, we induced pressure overload injury by performing transverse aortic constriction (TAC) surgery in SCOT-Heart-KO and αMHC-Cre control mice. While TAC increased left ventricular mass equally in both groups, at four weeks post-TAC, myocardial ROS abundance was increased in myocardium of SCOT-Heart-KO mice, and mitochondria and myofilaments were ultrastructurally disordered. Eight weeks post-TAC, left ventricular volume was markedly increased and ejection fraction was decreased in SCOT-Heart-KO mice, while these parameters remained normal in hearts of control animals.

**Conclusions:** These studies demonstrate the ability of myocardial ketone metabolism to coordinate the myocardial response to pressure overload, and suggest that the oxidation of ketone bodies may be an important contributor to free radical homeostasis and hemodynamic preservation in the injured heart.



**Keywords** Myocardial ketone body metabolism; Nuclear magnetic resonance (NMR) measurement of substrate metabolism; Ventricular remodeling; Oxidative stress; Mitochondrial metabolism

## 1. INTRODUCTION

During evolution of adverse ventricular remodeling that culminates in cardiomyopathy and congestive heart failure, myocardial fuel utilization becomes inefficient and inflexible, and mechanistic studies in pre-clinical models indicate that altered substrate and energy metabolism can cause cardiomyopathy [1—5]. Therefore, deeper understanding and ultimately, judicious nutritional and pharmacological manipulation of myocardial metabolism are expected to improve morbidity and mortality attributable to heart failure [6,7]. While the roles of the primary myocardial fuels, fatty acids and glucose, in myocardial homeostasis and disease have been explored extensively, the influence of myocardial ketone bodies, considered a secondary substrate class due to their low circulating concentrations in fed states, remains ill-defined. However, ketone bodies are highly competitive substrates for myocardial oxidative metabolism, and ketone bodies

[1]Department of Medicine, Center for Cardiovascular Research, Washington University, St. Louis, MO, USA [2]Department of Chemistry, Washington University, St. Louis, MO, USA [3]Department of Genetics, Washington University, St. Louis, MO, USA

*Corresponding author. Present address: Sanford-Burnham Medical Research Institute, 6400 Sanger Rd., Orlando, FL 32827, USA. Tel.: +1 407 745 2135. E-mail: pcrawford@sanfordburnham.org (P.A. Crawford).

Received July 3, 2014 • Revision received July 19, 2014 • Accepted July 23, 2014 • Available online 13 August 2014

http://dx.doi.org/10.1016/j.molmet.2014.07.010

 

circulate at increased concentrations in the setting of heart failure, at concentrations directly proportional to severity of the cardiomyopathy [8–10].

The liver is the source of the circulating ketone bodies D-β-hydroxybutyrate (D-βOHB) and acetoacetate (AcAc), whose myocardial oxidation requires the mitochondrial matrix enzyme succinyl-CoA:3-oxoacid-CoA transferase (SCOT, encoded by nuclear *Oxct1*), which as the only CoA transferase encoded by the mammalian genome, uniquely catalyzes a near-equilibrium reaction that transfers coenzyme A (CoA) between AcAc and succinate (see Ref. [11] for a recent review on integrated ketone body metabolism). Congenital and ubiquitous absence of SCOT causes significant morbidity in humans [12], and is incompatible with neonatal life in mice [13]. SCOT is absolutely required for terminal oxidation of ketone bodies [13], and through its ability to influence succinate metabolism, the reaction it catalyzes directly interfaces with the tricarboxylic acid (TCA) cycle and the electron transport chain [11]. Consequently its ability to influence myocardial bioenergetics may transcend physiological states considered 'ketotic'.

The heart is the highest ketone body consumer per unit mass, oxidizing ketone bodies in proportion to their delivery at the expense of fatty acid oxidation and glucose oxidation [14–19]. Compared with fatty acid oxidation, ketone bodies are more energetically efficient, yielding more energy available for ATP synthesis per molecule of oxygen invested [20–22]. Furthermore, the oxidation of ketone bodies may attenuate ROS production associated with the oxidation of fatty acids [21–23] suggesting that myocardial ketone body oxidation could protect against injury and adverse ventricular remodeling responses, which promote the development of cardiomyopathy and heart failure [24]. Indeed, clinical data suggest that myocardial ketone body metabolism may serve as an important therapeutic target. At least a subset of patients diagnosed with SCOT-deficiency exhibited dilated cardiomyopathy on presentation [25–28]. Moreover, extraction of delivered ketone bodies is maintained in failing hearts, but not skeletal muscle, of humans with advanced heart failure [29]. Similarly, the contribution of ketone bodies to cardiac energy metabolism may be elevated in patients with dilated and hypertrophic cardiomyopathies [30]. These results suggest that the diminution of myocardial fatty acid oxidation that typically occurs during the evolution of advanced cardiomyopathy may not be coupled to reduction of ketone body oxidation [1,2,5]. It is unclear whether maintained, or even elevated, utilization of ketone bodies preserves cardiac function, is a pathologic consequence, or is an innocent bystander in the adversely remodeling heart.

Therefore, mechanistic studies using tissue-selective genetic rodent models will begin to establish when and whether myocardial ketone body metabolism may be protective or deleterious to the heart. Here, we sought to investigate the role of ketone utilization in the heart during periods of myocardial stress by using mice with cardiomyocyte-specific loss of SCOT (SCOT-Heart-KO) to determine the physiological and pathological responses of myocardium lacking the ability to utilize ketones as an energy source.

## 2. MATERIALS AND METHODS

### 2.1. Animals and diets

The Animal Studies Committee at Washington University approved all experiments prior to their performance. SCOT-Heart-KO mice were generated by successive generations of breeding of *Oxct1*$^{flox/flox}$ mice to mice expressing Cre recombinase under control of the alpha myosin heavy chain promoter (αMHC-Cre, Jackson Laboratory, stock number 011038) [31]. SCOT-Heart-KO and αMHC-Cre control mice (male mice were studied) were maintained for at least ten generations on a C57BL/6N × C57BL/6J hybrid substrain background. A few experiments were performed using a tamoxifen inducible SCOT-Heart-KO strain that was generated by breeding *Oxct1*$^{flox/flox}$ mice to mice expressing tamoxifen inducible Cre recombinase under control of the αMHC promoter (MerCreMer, Jackson Laboratory, stock number 005657). To induce knockdown of SCOT in the cardiomyocytes of adult mice, tamoxifen (20 mg/kg) was administered intraperitoneally for 21 d. Mice were maintained on Lab Diet (5053) *ad libitum* and autoclaved water on cedar chip bedding at 22 °C. Lights were off between 1800 and 0600. Food was removed and fresh bedding was provided at the onset of fasting for mice fasted for 24 h; water was provided *ad libitum* to fasting animals. For some studies, mice were maintained on a rodent ketogenic diet (Harlan-Teklad TD.110633), which was described previously in Ref. [32] and is comprised of 94.1% fat, 4.6% protein, and 1.3% carbohydrate. The contributing fat sources are lard and milkfat; casein is the protein source, and sucrose is the minimal carbohydrate source; the diet is deficient in choline. A cohort of mice was also maintained on a 40% fat diet (Harlan-Teklad TD.110290), which is comprised of 40.7% fat, 40.3% carbohydrate, and 19% protein, in which lard and milkfat are the fat sources, casein is the protein source, and sucrose (18.3% by mass) and cornstarch are the carbohydrate sources.

### 2.2. Metabolite and insulin measurements

Serum samples were acquired from animals that had been fasted for 4 h on fresh cedar chip bedding. Serum glucose, D-βOHB, total ketone bodies (TKB, D-βOHB plus AcAc), triacylglycerols (TAG), and insulin concentrations were measured as previously described in Ref. [33].

### 2.3. Langendorff heart perfusions

Mouse heart perfusions were performed as previously described in Ref. [33]. Briefly, SCOT-Heart-KO and αMHC-Cre mice received 100 units of heparin by intraperitoneal injection and 10 min later were anesthetized with an intraperitoneal injection of 390 mg/kg sodium pentobarbital. Hearts were excised and placed in ice-cold Krebs-Henseleit (KH) bicarbonate solution (118 mM NaCl, 25 mM $NaHCO_3$, 4.7 mM KCl, 0.4 mM $KH_2PO_4$, 2.5 mM $CaCl_2$, pH 7.4) supplemented with 5 mM glucose. Hearts were cannulated *via* the aorta and then perfused in the Langendorff mode at a constant pressure of 60 mmHg, with continuous bubbling of a 95% $O_2$/5% $CO_2$ gas mixture into the KH-bicarbonate buffer with 3% fatty acid free bovine serum albumin (BSA). Experimental perfusion conditions are described in the legends for Figures 1 and 2. Insulin used for all perfusions was human insulin (rDNA origin; Lilly).

### 2.4. NMR spectroscopy of myocardial extracts

After 20 min of perfusion, freeze-clamped (liquid $N_2$-cooled tongs) hearts were homogenized in 3.6% perchloric acid, followed by removal of precipitated debris and pH neutralization of the supernatant with KOH. Neutralized perchloric acid tissue extracts were dissolved in 310 μL of $D_2O$ (Cambridge Isotope Laboratories) spiked with 1 mM trimethylsilyl propionate (TSP), which provides a chemical shift reference and an internal concentration standard to quantify extract metabolite concentrations. Extracts were transferred into thin-walled 5 mm NMR tubes (Shigemi) and profiled using $^{13}C$-edited proton nuclear magnetic resonance (NMR) measured at 11.75 T (Varian/Agilent Direct Drive-1) *via* first increment gradient heteronuclear single-quantum correlation (gHSQC) as previously described in Refs. [13,31,33,34], obtaining integrals for carbon #4 of glutamate, carbon #2 of taurine, carbon #3 of lactate, carbons #2/#3 of succinate, carbon

 

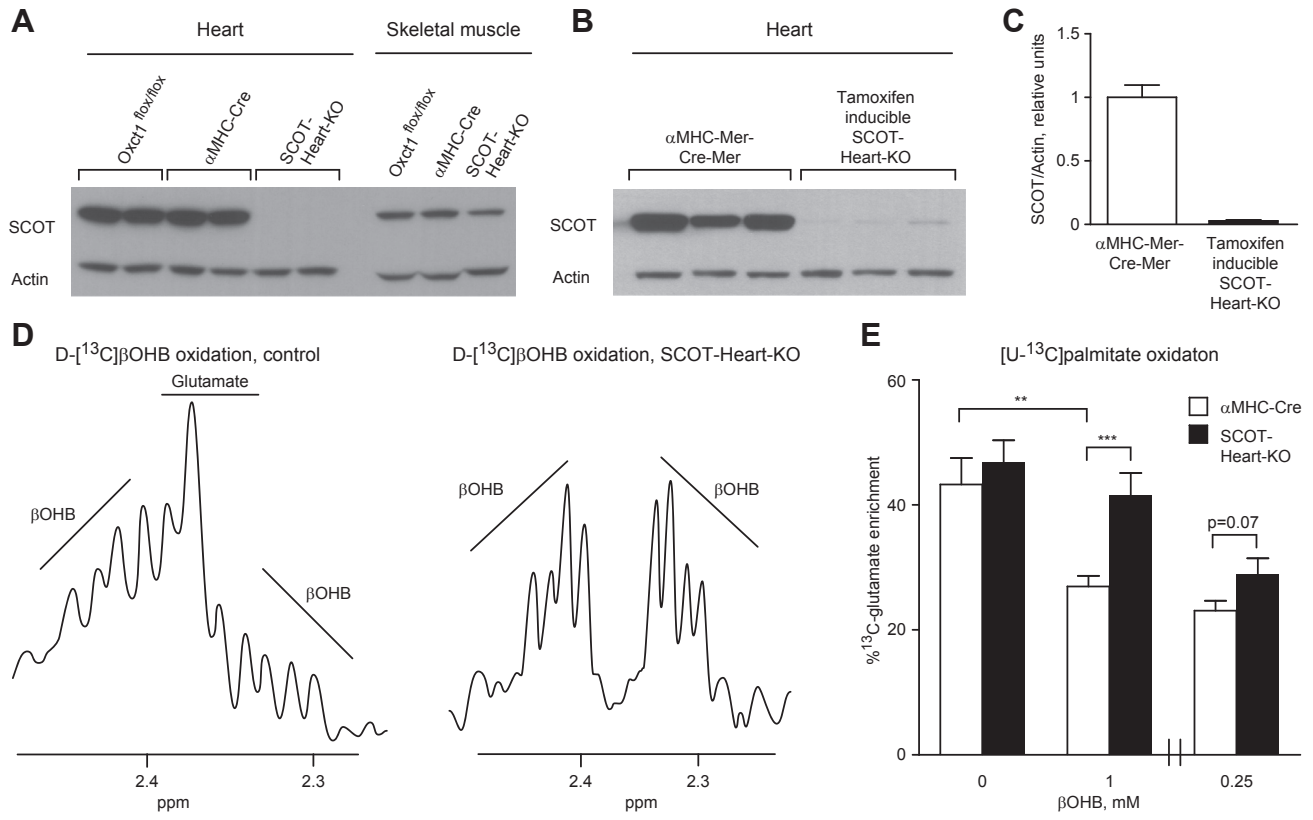


**Figure 1:** Myocardial SCOT expression is required for ketone body oxidation. (A) Immunoblot for ketolytic enzyme succinyl-CoA:3-oxoacid-CoA transferase (SCOT) and actin in heart and skeletal muscle protein lysates derived from adult αMHC-Cre, *Oxct1*$^{flox/flox}$, and SCOT-Heart-KO mice. Immunoblot (B) and quantification (C) for ketolytic enzyme succinyl-CoA:3-oxoacid-CoA transferase (SCOT) and actin in heart protein lysates derived from adult αMHC-MerCreMer and tamoxifen-inducible SCOT-Heart-KO mice following intraperitoneal injections of 20 mg/kg tamoxifen for 21 d. (D) $^{13}$C-edited proton NMR spectrum (2.1—2.5 ppm, relative to chemical shift of trimethylsilyl propionate internal standard) from hearts of αMHC-Cre and SCOT-Heart-KO mice that had been perfused with a buffer containing 11 mM glucose, 20 μU/mL insulin, 0.6 mM palmitate, and 1 mM sodium D-[2,4-$^{13}C_2$]βOHB for 15 min prior to collection of tissues and generation of extracts. $^{13}$C-Glutamate is a reporter of the contribution of $^{13}$C-labeled D-βOHB to TCA cycle flux, and is selectively absent in myocardial extracts from SCOT-Heart-KO mice. (E) Fractional $^{13}$C-enrichment of glutamate (a surrogate for the contribution of a $^{13}$C-labeled substrate to the TCA cycle) in hearts of αMHC-Cre and SCOT-Heart-KO mice perfused *ex vivo* with a buffer containing either (i) 1.2 mM [U-$^{13}$C]palmitic acid, 5 mM glucose, 1 μU/mL insulin, 1 mM lactate and 0 mM or 1 mM unlabeled D-βOHB, or (ii) 0.6 mM [U-$^{13}$C]palmitic acid, 11 mM glucose, 10 μU/mL insulin, 1 mM lactate and 0.25 mM unlabeled D-βOHB measured by $^{13}$C-edited proton NMR. $n = 4$—9 mice/group. $^{**}p \leq 0.01$, $^{***}p \leq 0.001$ by 1-way ANOVA with Tukey's post hoc analysis.

#3 of alanine, and carbon #6 of 2-deoxyglucose-6-phosphate. For quantification of $^{13}$C-enrichment of carbons #1 and #5 of glutamate from [1-$^{13}$C]acetate (Figure 2I), band-selective heteronuclear multiple quantum coherence (HMBC) experiments were carried out on heart tissue extracts following perfusion. Samples were prepared by dissolving dried extracts in 280 μL of $D_2O$ followed by pH correction to near 7.0 by addition of KOH. The extract solutions were charged into 5 mm matched susceptibility plug Shigemi tubes prior to analysis, and data were collected at 25 °C. Experiments were configured to selectively monitor two-bond $^{1}$H—$^{13}$C correlations between glutamate carbon position #4 and #2 proton signals and #5 and #1 carbonyl carbons. The carbon chemical shift (F1 domain) selectivity was accomplished through use of adiabatic pulses and limited to 2011 Hz. Proton acquisition in t2 was carried out for 255 ms over a spectral width of 2376 Hz resulting in 606 complex data points. Adequate resolution was obtained using 32 t1 increments collected in phase-sensitive mode coupled with linear prediction in F1 prior to Fourier transformation (2048 × 256; t2 × t1). Adequate signal-to-noise was obtained from 24 transients on all extract samples. Additional collection conditions include delay times of 12 s between transients, $^{1}$H 90-degree pulse of 8 μs, $^{13}$C 90-degree pulse of 12 μs and coherence delay time of 50 ms corresponding to a two-bond H—C coupling of 10 Hz. These conditions for glutamate result in a 2-to-1 proton receptivity for the volume integrals resulting from glutamate carbon positions #4 and #2, respectively, for equal $^{13}$C labeling on glutamate carbon positions #5 and #1.

### 2.5. Lipopolysaccharide (LPS) injections

SCOT-Heart-KO and αMHC-Cre mice were given intraperitoneal injections of 8 mg/kg of *Escherichia coli* 0111:B4 LPS (Sigma) suspended in phosphate-buffered saline (PBS). Control cohorts received an injection of an equal volume of PBS alone. Injections were performed in the morning, and food was removed from all animals immediately after the injections. At 6 h post-injection, LPS-induced cardiac dysfunction was assessed by echocardiography. A separate cohort of mice was used for serum analysis and tissue collection at 6 h post-injection.

### 2.6. Transverse aortic constriction (TAC)

Surgeries were performed as described previously in Ref. [35,36]. Briefly, mice were anesthetized with ketamine (100 mg/kg) and xylazine (10 mg/kg) administered IP, and surgery was performed using aseptic technique. Each mouse was restrained supine on a magnetic stainless steel surgical board with warmer attached. Following blunt

 

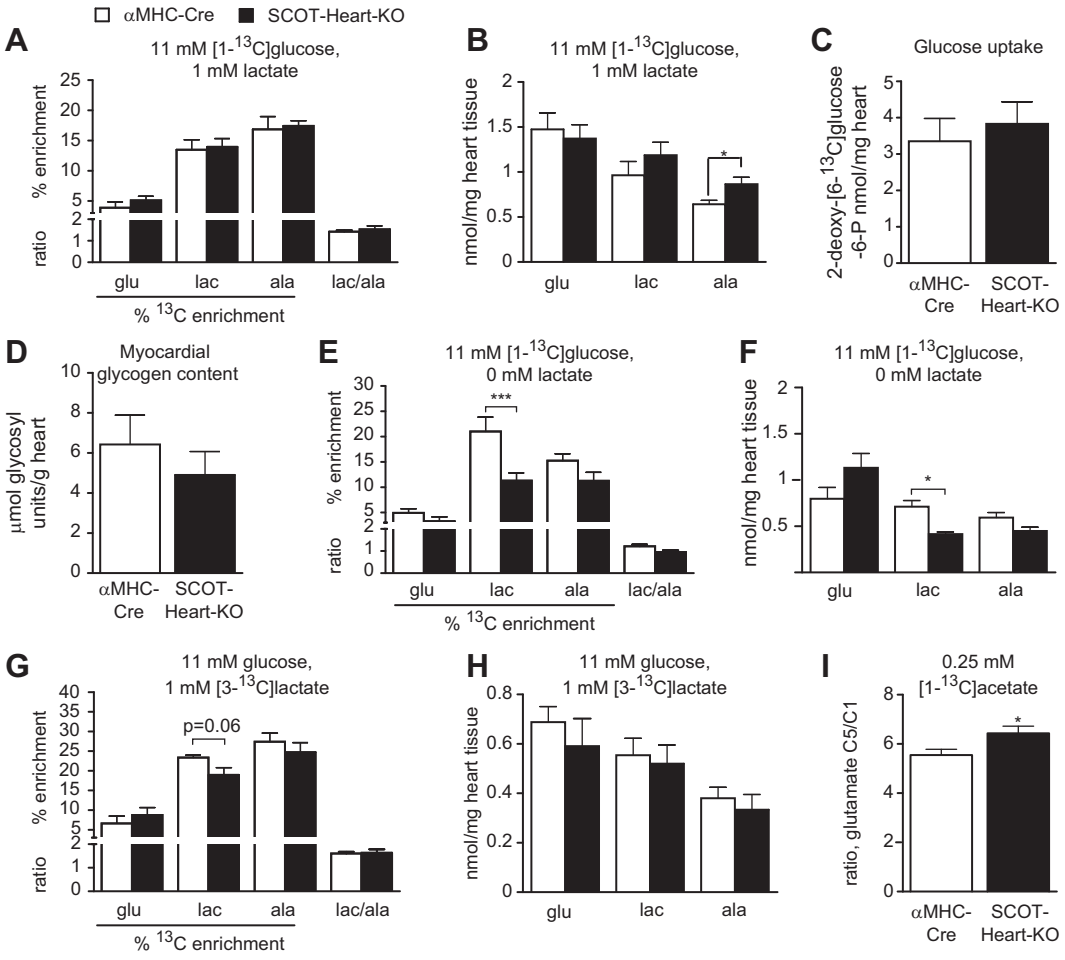


**Figure 2:** Reconfigured metabolism in the absence of myocardial SCOT. (A, B) Fractional % $^{13}$C-enrichment of glutamate (glu), lactate (lac), and alanine (ala) or absolute pools of metabolites (nmol/mg tissue) in hearts of αMHC-Cre control and SCOT-Heart-KO mice perfused *ex vivo* with a buffer containing 11 mM [1-$^{13}$C]glucose, 20 μU/mL insulin, 0.6 mM palmitate, 0.25 mM D-βOHB and 1 mM sodium lactate measured by $^{13}$C-edited proton NMR. (C) Myocardial glucose uptake measured by perfusing hearts with a buffer containing 1 mM [6-$^{13}$C]-deoxyglucose, 20 μU/mL insulin, 0.6 mM palmitate and 1 mM sodium lactate and the phosphorylation of 2-deoxy-[6-$^{13}$C]glucose was detected by $^{13}$C-edited proton NMR. (D) Myocardial glycogen content. (E, F) Fractional $^{13}$C-enrichment of glutamate, lactate, and alanine (%), or total pools of metabolites (nmol/mg tissue) in hearts following perfusion with 11 mM [1-$^{13}$C] glucose, 20 μU/mL insulin, 0.6 mM palmitate and 0.25 mM D-βOHB, and 0 mM lactate; or (G, H) 11 mM glucose, 20 μU/mL insulin, 0.6 mM palmitate, 0.25 mM D-βOHB and 1 mM sodium [3-$^{13}$C]-lactate measured by $^{13}$C-edited proton NMR. (I) A surrogate for anaplerosis was acquired by perfusing hearts with a buffer containing 11 mM glucose, 10 μU/mL insulin, 0.6 mM palmitate, 0.25 mM D-βOHB, 1 mM lactate and 0.25 mM sodium [1-$^{13}$C]-acetate. $n = 5$–10 mice/group. $^{*}p \leq 0.05$, $^{***}p \leq 0.001$ by 1-way ANOVA with Tukey's post hoc test.

dissection through the intercostal muscles, the aorta was identified and freed by additional blunt dissection. 7.0 silk suture was placed around the transverse aorta and tied tightly around a blunt needle (27 gauge). The needle was then rapidly removed and the chest wall was closed using a purse string suture. The surgical incision was closed in two layers with an interrupted suture pattern. The mouse was kept warm on a heating pad throughout the procedure and during recovery. Sham-operated mice received the same surgery, except that the suture was simply placed around the aorta briefly, but not tied. At 4 wk or 8 wk post-surgery, cardiac function was assessed by echocardiography. At the end of the study, mice were euthanized by $CO_2$ inhalation followed by cervical dislocation; hearts were removed rapidly and snap frozen in $LiN_2$.

### 2.7. Echocardiography

Echocardiography was performed using a Vevo 2100 Imaging System (VisualSonics, Toronto, Canada) equipped with a 30 MHz linear-array transducer. Parasternal long-axis views were obtained by a handheld technique under 1–2% isofluorane (fasting and lipopolysaccharide studies), or 100 mg/kg tribromoethanol (ketogenic diet, high fat diet, sham operated, 4 wk, and 8 wk TAC studies) anesthetic conditions. Two-dimensional and M-mode images were obtained in the long- and short-axis views to calculate fractional shortening (FS). Quantitative image analysis was also performed using a speckle-tracking algorithm. In brief, suitable 2-D cine-loops were selected from digitally acquired echocardiographic images based on adequate visualization of the endo- and epicardial border and absence of image artifacts. Three consecutive cardiac cycles were selected for analysis based on image quality. Semi-automated tracing of the endocardial and epicardial borders were performed and verified over all 3 cardiac cycles and then corrected as needed to achieve good quality tracking throughout each cine loop. Tracked images were then processed in a frame-by-frame manner to derive the following parameters: left ventricular (LV) volumes (end-diastolic and end-systolic, calculated by the disk summation method); rate-of-change of LV volumes (peak positive and peak-negative); stroke volume (end-diastolic volume minus end-

 

systolic volume), ejection fraction (stroke volume divided by end-diastolic volume multiplied by 100); LV mass (volume of the epicardial shell minus volume of the endocardial shell multiplied by the specific gravity of muscle); and global radial myocardial strain (averaged peak segmental radial strain).

### 2.8. Immunoblot

Protein extracts were prepared in a buffer consisting of 20 mM Tris, 150 mM NaCl, 1 mM EDTA, 1% Triton-X 100, protease inhibitors (Roche), and phosphatase inhibitors (Sigma), as previously described in Ref. [19]. Immunoblots measuring myocardial carbonylated proteins were measured using the OxyBlot Protein Oxidation Kit (Millipore). MitoProfile total OXPHOS antibody cocktail (abcam) was used to measure key proteins of the electron transport chain. Acetylated lysine antibody (Cell Signaling) was used to measure acetylated lysine residues in myocardial and mitochondrial extracts, and succinylated lysine antibody (PTM Biolab) was used to measure succinylated lysine residues in myocardial extracts. Band intensities were densitometrically quantified using QuantityOne software. For myocardial extracts prepared for acetylated lysine, the extract was prepared in the above buffer with the addition of 1 μM trichostatin A, and 50 μM Sirtuin inhibitor AGK7.

### 2.9. Histology and transmission electron microscopy (TEM)

Hearts from SCOT-Heart-KO and αMHC-Cre mice after 4 wk TAC ($n = 2$/group) were fixed in a modified Karnovsky's fixative of 3% glutaraldehyde and 1% paraformaldehyde in 0.1 M sodium cacodylate buffer for at least 24 h, followed by a post-fix in 2% osmium tetroxide in 0.1 M sodium cacodylate buffer for 1 h prior to en bloc staining with 2% aqueous uranyl acetate for 30 min, dehydration in graded ethanols and embedding in PolyBed 812 (Polysciences, Hatfield, PA). Tissue blocks were sectioned at 90 nm thickness, then stained with Venable's lead citrate and viewed with a JEOL model 1400EX electron microscope (JEOL, Tokyo). Digital images were acquired using the Gatan Orius (Gatan, Warrendale, PA) high definition CCD, 11 megapixel TEM camera.

For light microscopy, hearts were collected from mice immediately post-sacrifice and fixed in 10% neutral buffered formalin. Tissue was embedded in paraffin, microtome-sectioned, stained with hematoxylin and eosin, and imaged using a Zeiss Axioskop microscope and AxioVision software (version 4.7, San Diego, CA).

### 2.10. Mitochondrial isolation

Whole hearts were excised, washed, atria were removed, and ventricular tissue minced on ice as previously described in Ref. [19]. Mitochondrial isolation medium (MIM; 300 mM sucrose, 0.2 mM EDTA, 10 mM Na HEPES, pH 7.4) and bovine pancreatic trypsin [0.125 mg/mL trypsin; specific activity ≥ 9000 Na-Benzoyl-L-Arginine Ethyl Ester (BAEE) units/mg protein; Sigma] was added to digest the tissue for 15 min at 4 °C, followed by the addition of equal volumes MIM containing BSA (1 mg/mL) and soybean trypsin inhibitor (0.65 mg/mL) to halt the digestion. The samples were then rapidly homogenized on ice by using a Glas-Col dounce homogenizer, and centrifuged at 600 × *g* for 10 min at 4 °C in MIM buffer containing BSA (MIM-BSA; 1 mg/mL). The resulting supernatant, which contained mitochondria, was spun at 8000 × *g* for 15 min at 4 °C, the supernatant discarded, the mitochondrial pellet re-suspended in 10 mL of ice-cold MIM + BSA, and the sample centrifuged again at 8000 × *g* for 15 min at 4 °C. The pellet was briefly washed in ice-cold MIM and each tissue sample was resuspended in 75 μL of ice-cold MIM (pH 7.2). For mitochondria isolated for immunoblots, the final pellet was resuspended in 75 μL of protein lysis buffer containing protease inhibitors, phosphatase inhibitors, 1 μM trichostatin A, and 50 μM Sirtuin inhibitor AGK7.

### 2.11. Mitochondrial respiration

Immediately following mitochondrial isolation, total protein was quantified by Bradford assay (Bio-Rad). Respiration was quantified at 37 °C using a water-jacketed Clark Electrode (Hansatech Instruments) under conditions described previously in Ref. [37]. Briefly, 0.5 mg of mitochondria were added to 1 mL of respiration buffer [125 mM KCl, 20 mM HEPES, 3 mM Mg-acetate, 0.4 mM EGTA, 0.3 mM dithiothreitol (DTT), 5 mM $KH_2PO_4$, 0.2% BSA, pH 7.1] containing either 20 μM palmitoyl-L-carnitine and 5 mM malate or 5 mM succinate and 10 μM rotenone. The solubility of oxygen in the respiration buffer at 37 °C was 235 nmol $O_2$ per mL. Following measurement of basal (state 2) respiration, 1 mM ADP was added to the respiration chamber, and maximal (state 3) respiration quantified. Thereafter, state 4 ($F_1F_0$ ATPase-independent) respiration was measured by adding 1 μg/mL oligomycin (Sigma) to inhibit $F_1F_0$ ATP synthase. Uncoupled respiration was measured following the addition of 5 μM carbonyl cyanide 4-(trifluoromethoxy)phenylhydrazone (FCCP) where applicable.

### 2.12. Tissue triglyceride, glycogen, and nicotinamide metabolite quantifications

Myocardial triglycerides, using a Folch extract of heart and biochemical quantification, were quantified as previously described in Ref. [19]. Myocardial glycogen and $NAD^+$(H) concentrations were measured in heart lysates using fluorescent biochemical assays (Biovision).

### 2.13. Quantification of $H_2O_2$ production

Mitochondria were added to an incubation buffer containing 125 mM KCl, 4 mM $KH_2PO_4$, 20 mM HEPES, pH 7.2, 1 mM $MgCl_2$, 0.2% fatty acid free bovine serum albumin, and 20 μM EGTA, as well as 100 μM Amplex® Red and 100 mU horseradish peroxidase (Amplex® Red Hydrogen Peroxide/Peroxidase Assay Kit, Invitrogen), and fluorescence was measured (Ex 560 nm, Em 590 nm). After several baseline acquisitions, sodium succinate was added to a final concentration of 10 mM to induce $H_2O_2$ production. Other substrate combinations included 10 mM succinate plus 1 mM D-βOHB, and 10 mM succinate plus 1 mM AcAc (base hydrolyzed from ethyl AcAc, see Ref. [34] for details). After 5 min, 0.5 μM rotenone was added to attenuate $H_2O_2$ production from reverse electron transport.

### 2.14. CellROX quantification of tissue superoxide

The CellROX® Green reagent detects superoxide localized within the mitochondria and nuclei by binding to DNA after reacting with superoxide, while CellROX® Deep Red reagent detects ROS localized in the cytoplasm in living cells, and total tissue superoxide content in fresh tissue harvested from the animal. CellROX® quantification of tissue superoxide levels were performed in fresh-frozen (in Optimal Cutting Temperature medium) left ventricular cryosections following incubation for 30 min at 37 °C using a final concentration of each CellROX® dye of 5 μM ($n = 3$ hearts/condition). All slides were examined and images were acquired at 0.5 μm slice thickness using a Zeiss LSM 700 confocal microscope and Zeiss Zen software. All images were acquired using the same gain measurement. Using ImageJ, CellROX® intensity was quantified in at least 3 × 20× fields per mouse.

### 2.15. Statistical analyses

Analyses were performed with GraphPad 5.0 software (Prism, San Diego, CA), using tests described within the text and figure legends.

 

## 3. RESULTS

### 3.1. Remodeled substrate preference and intermediary metabolism in hearts of SCOT-Heart-KO mice

Despite increased ketone body delivery in mice maintained on a high fat, low carbohydrate ketogenic diet, myocardial expression of the enzyme uniquely required for ketone body oxidation, succinyl-CoA:3-oxoacid-CoA transferase (SCOT), and intrinsic myocardial capacity to oxidize ketone bodies are surprisingly both decreased [33]. Furthermore, the normal ability of ketone bodies to suppress myocardial fatty acid oxidation is abrogated [33]. To determine whether diminished ketolytic capacity during periods of increased ketosis confers salutary or detrimental hemodynamic effects, *in vivo* hemodynamic function was quantified by echocardiography in wild-type mice maintained on a commonly studied ketogenic diet for 4 wk (Table 1). In accordance with our previous studies [32,33], serum D-βOHB concentrations were elevated nearly 10-fold by ketogenic diet feeding, compared with mice fed standard chow, and normal weight gain in chow-fed mice was attenuated by the ketogenic diet. While no overt alterations in cardiac hemodynamic function were detected in ketogenic diet-fed mice, echocardiographic analysis revealed several modest but significant alterations including reduced heart rate and a concomitantly increased left ventricular ejection time (Table 1). Indeed, D-βOHB has been demonstrated to decrease sympathetic outflow and may explain the reduced heart rate of mice maintained on this ketogenic diet [38].

While this experiment demonstrates the absence of deleterious hemodynamic effects of ketogenic diet-induced partial impairment of ketolytic capacity, the hemodynamic and metabolic effects of complete loss of the ability to metabolize ketone bodies in the heart have not been determined. In the mouse heart this may be particularly important, because as much as 34% of myocardial oxidative metabolism proceeds through ketone body oxidation [39]. Because germline deletion of SCOT results in neonatal lethality [13], mice with cardiomyocyte-specific loss of SCOT (SCOT-Heart-KO) were developed using an αMHC-Cre driver strain [31]. SCOT-Heart-KO mice are viable and lack SCOT protein and enzyme activity specifically in the myocardium, while SCOT is retained in other ketolytic tissues such as skeletal muscle (Figure 1A). Because αMHC gene expression is activated during embryonic development [40], phenotypes of adult SCOT-Heart-KO mice may be muted by compensatory metabolic changes elicited in the developmental or neonatal stages, and thus a tamoxifen-inducible SCOT-Heart-KO mouse strain was also generated by crossing *Oxct1*$^{flox/flox}$ mice to the αMHC-MerCreMer transgenic strain to explore the effects of SCOT deficiency following deletion in adult mice for a subset of experiments (Figure 1B,C, Table 2).

Using *ex vivo* Langendorff heart perfusions and $^{13}$C-edited proton nuclear magnetic resonance (NMR) spectroscopy, we confirmed that hearts of adult SCOT-Heart-KO mice are unable to terminally oxidize D-[$^{13}$C]βOHB (Figure 1D). Moreover, suppression of the contribution of $^{13}$C-labeled fatty acid-derived acetyl-CoA to the tricarboxylic acid (TCA) cycle by ketone bodies is abrogated in perfused hearts of SCOT-Heart-KO mice, indicating unrestrained fatty acid oxidation under perfusion conditions mimicking both the fed (0.25 mM D-βOHB) and fasted (1 mM D-βOHB) states (Figure 1E). $^{13}$C-labeled glucose metabolism was also quantified in hearts of SCOT-Heart-KO mice using perfusion buffers in the presence of the anaplerotic (*i.e.*, intermediates supplied to the TCA cycle independent of citrate synthase) substrate lactate (1 mM). The procession of glucose through glycolysis yields pyruvate, which is predominantly channeled *via* (i) decarboxylation by pyruvate dehydrogenase, forming acetyl-CoA for entry into the TCA cycle *via* citrate synthase, (ii) carboxylation, forming the TCA cycle intermediate malate or oxaloacetate (anaplerotic reactions catalyzed by malic enzymes and pyruvate carboxylase, respectively), (iii) reduction to lactate *via* lactate dehydrogenase, a reversible NAD$^+$/NADH-coupled redox reaction, or (iv) transamination to alanine. Compared to hearts of αMHC-Cre control mice, no differences in $^{13}$C-enrichment of glutamate from [1-$^{13}$C]glucose (fractional $^{13}$C-enrichment of glutamate serves as a quantitative surrogate for [$^{13}$C]acetyl-CoA procession through citrate synthase [41]) were observed, nor were there differences in the $^{13}$C-enrichments of lactate or alanine (Figure 2A). While extracts derived from perfused hearts from SCOT-Heart-KO mice exhibited modestly larger alanine pools (Figure 2B), no differences in relative lactate/alanine ratios were observed, suggesting normal NAD$^+$/NADH redox couple balance in hearts of SCOT-Heart-KO mice under these perfusion conditions. Loss of SCOT did not influence glucose uptake, as measured by accumulation of phosphorylated 2-deoxy-[6-$^{13}$C]glucose, or baseline steady-state glycogen content (Figure 2C, D).

To determine if lactate included in the perfusion buffer concealed metabolic reprogramming in the SCOT-Heart-KO heart, [1-$^{13}$C]glucose was perfused in the absence of exogenous unlabeled lactate. While $^{13}$C-enrichment of glutamate remained normal in hearts of SCOT-Heart-KO mice (Figure 2E), SCOT deficiency in myocardium was associated with a significant attenuation in *de novo* formation of $^{13}$C-lactate. Total endogenous myocardial lactate pools were also lower in SCOT-Heart-KO mice under these perfusion conditions, while lactate/alanine ratios remained normal (Figure 2F). To determine if the decreased lactate abundance in hearts of SCOT-Heart-KO mice was associated with increased lactate oxidation, we performed parallel perfusions in which the buffer components were identical to previous perfusions that included 1 mM lactate, but in which [3-$^{13}$C]lactate was used instead of unlabeled lactate, and unlabeled glucose was used instead of [1-$^{13}$C]glucose. No differences in fractional $^{13}$C-enrichment of glutamate from [3-$^{13}$C]lactate were observed, suggesting that the oxidation of lactate is similar between SCOT-Heart-KO and αMHC-Cre mice (Figure 2G). Taken together, given decreased channeling of glucose metabolites to lactate, only in the absence of exogenous lactate, these results suggest that hearts of SCOT-Heart-KO mice may be particularly poised to channel lactate-derived pyruvate to anaplerosis.

**Table 1** — Echocardiographic and metabolic responses of wild-type mice following 4 wk on ketogenic diet.

| | Chow | Ketogenic Diet |
|---|---|---|
| Serum D-βOHB, mM | 0.17 ± 0.03 | 1.81 ± 0.50** |
| Body weight, g, initiation of study | 20.5 ± 0.5 | 20.8 ± 0.8 |
| Body weight, g, after 4 wk on diet | 22.9 ± 0.9 | 18.9 ± 1.3* |
| Heart rate, bpm | 488 ± 16.6 | 414 ± 17.8* |
| LVIDd, mm | 3.98 ± 0.06 | 3.82 ± 0.07 |
| LVIDs, mm | 2.92 ± 0.05 | 2.74 ± 0.11 |
| LVMI, mg/mm tibial length | 5.08 ± 0.19 | 4.77 ± 0.39 |
| E, mm/s | 641 ± 22.9 | 687 ± 42.8 |
| A, mm/s | 537 ± 25.1 | 453 ± 45.7 |
| E/A | 1.20 ± 0.04 | 1.57 ± 0.16* |
| DT, ms | 20.3 ± 2.1 | 20.2 ± 1.5 |
| IVRT, ms | 15.2 ± 0.6 | 16.6 ± 1.1 |
| E′, mm/s | 22.9 ± 1.2 | 19.5 ± 1.6 |
| A′, mm/s | 22.8 ± 1.09 | 16.0 ± 1.03** |
| E/E′ | 28.4 ± 2.1 | 35.8 ± 2.4* |
| FS, % | 0.27 ± 0.01 | 0.28 ± 0.02 |
| S′, mm/s | 15.7 ± 1.1 | 15 ± 1.0 |
| IVCT, ms | 11.0 ± 0.8 | 11.6 ± 1.7 |
| ET, ms | 43.4 ± 0.5 | 48.9 ± 0.6*** |

*$p \leq 0.05$; **$p \leq 0.01$; ***$p \leq 0.001$. $n = 5$/group.

 

**Table 2** — Echocardiographic analysis post-metabolic stress.

| | Baseline | | 24 h Fast | | 24 h Fast Tamoxifen-inducible | | Lipopolysaccharide | |
|---|---|---|---|---|---|---|---|---|
| Genotype | αMHC-Cre | SCOT-Heart-KO | αMHC-Cre | SCOT-Heart-KO | αMHC-MerCreMer | TamInd-SCOT-Heart-KO | αMHC-Cre | SCOT-Heart-KO |
| Heart rate, bpm | 517.8 ± 39.4 | 471.2 ± 15.2 | 451.6 ± 11.0 | 434.4 ± 5.6 | 461.8 ± 13.2 | 407.4 ± 10.3* | 556.7 ± 9.7 | 581.5 ± 22.2## |
| LVIDd, mm | 4.0 ± 0.2 | 4.2 ± 0.1 | 3.9 ± 0.1 | 4.0 ± 0.1 | 4.2 ± 0.1 | 4.2 ± 0.1 | 3.5 ± 0.1 | 3.7 ± 0.1## |
| LVMI, mg/g body weight | 4.0 ± 0.1 | 4.2 ± 0.4 | 4.3 ± 0.2 | 4.3 ± 0.1 | 5.1 ± 0.3 | 5.1 ± 0.2 | 4.1 ± 0.2 | 4.2 ± 0.1 |
| FS, % | 30.2 ± 1.1 | 27.3 ± 1.1 | 31.4 ± 2.5 | 28.8 ± 1.7 | 25.0 ± 2.4 | 24.4 ± 1.5 | 27 ± 1.6 | 22.3 ± 1.6*,# |

*$p < 0.05$ compared to control group, same condition.
#$p < 0.05$ compared to baseline condition, same genotype.
##$p < 0.01$ compared to baseline condition, same genotype.
$n = 5$–6/group.

Therefore, to quantify whether the SCOT deficiency is associated with altered anaplerosis, hearts were perfused with [1-$^{13}$C]acetate, and positional enrichment of glutamate was quantified. [1-$^{13}$C]acetate labels glutamate on carbon position #5 during the first turn of the TCA cycle, and carbon position #1 on subsequent turns of the TCA cycle, but $^{13}$C-enrichment on carbon #1 is diluted in proportion to the magnitude of TCA cycle anaplerosis [42]. SCOT deficiency in the myocardium was associated with a significantly increased ratio of carbon #5/carbon #1, suggesting an increased rate of anaplerosis in hearts of SCOT-Heart-KO mice under baseline perfusion conditions (Figure 2I). No differences in abundances of mRNA transcripts for anaplerotic enzymes pyruvate carboxylase or the three malic enzymes were observed (data not shown).

### 3.2. Normal hemodynamic responses to ketosis in SCOT-Heart-KO mice

Acutely, cardiomyocytes oxidize ketone bodies in proportion to their delivery, at the expense of fatty acid oxidation and glucose oxidation. Because SCOT-Heart-KO mice exhibit increased contribution from fatty acids to the TCA cycle, we determined the impact of SCOT deficiency in the myocardium in the setting of fasting, a state in which glucose availability decreases, delivery of ketone bodies to the myocardium increases, and myocardial lipid delivery and storage increases [43]. Following a 24 h fast, no alterations of systolic function were observed in SCOT-Heart-KO mice (Table 2), and fasting to 48 h failed to reveal any difference in myocardial triglyceride content between SCOT-Heart-KO mice and αMHC-Cre controls (1.32 ± 0.4 and 1.33 ± 0.2 μg/mg of tissue, respectively). While a modest reduction in heart rate was observed in tamoxifen-inducible SCOT-Heart-KO mice that were fasted for 24 h, no differences in fractional shortening or LV mass were observed (Table 2).

To determine if more prolonged ketosis could induce significant adverse remodeling in hearts that lacked the ability to oxidize ketone bodies, we fed αMHC-Cre control and SCOT-Heart-KO mice a ketogenic diet for 12 wk. Heart weights, normalized to tibia length, were normal in SCOT-Heart-KO mice maintained on this diet, and serum ketone and glucose concentrations were unchanged compared to ketogenic diet-fed control mice (Supplemental Table 1). To determine if an adverse myocardial response to ketosis in SCOT-Heart-KO could be triggered by preceding caloric overload and weight gain, αMHC-Cre control and SCOT-Heart-KO mice were maintained on a sucrose-enriched 40% fat diet for 12 wk, and then switched to a ketogenic diet for 6 wk. As expected, the calorically enriched diet caused a marked weight gain in both groups, and the transition to the ketogenic diet caused a marked and equal weight loss between groups. Heart weights, normalized to tibia length, were normal in SCOT-Heart-KO mice following adherence to this diet, and serum ketone and glucose concentrations were not different between αMHC-Cre control and SCOT-Heart-KO mice (Supplemental Table 1), indicating that ketosis is well-tolerated by the heart even when ketone body oxidation is abrogated.

### 3.3. Myocardial stress induces structural and hemodynamic abnormalities in hearts of SCOT-Heart-KO mice

Because of (i) the successful adaptation of SCOT-Heart-KO mice to ketotic intervals that are normally associated with increased myocardial fatty acid and ketone body oxidation, and (ii) the increased fractional contribution of fatty acid oxidation to energy economy in the hearts of these knockout animals, we hypothesized that the pre-existing reliance on fatty acids for bioenergetic needs in hearts of SCOT-Heart-KO mice may cause an adverse response to conditions that normally cause the heart to become less reliant on fat oxidation and more dependent on glucose utilization. A robust mediator of the systemic inflammatory response, lipopolysaccharide (LPS), normally suppresses myocardial fatty acid oxidation and promotes cardiac dysfunction [44]. After LPS administration to SCOT-Heart-KO and αMHC-Cre control mice, echocardiography revealed that SCOT-Heart-KO mice exhibited moderately impaired fractional shortening at 6 h post-injection compared to LPS-injected αMHC-Cre control mice and to saline-injected SCOT-Heart-KO mice (Table 2), suggesting that SCOT-Heart-KO mice may have an impaired ability to adapt to pathological conditions that decrease fatty acid oxidation.

A common injurious myocardial stress is sustained hypertension, which in mice is experimentally mimicked by provoking cardiac pressure overload through surgical transverse aortic constriction (TAC). This procedure provokes metabolic abnormalities that precede and drive adverse ventricular remodeling [5,45]. To determine the effect of SCOT deficiency on pathological remodeling in response to pressure overload, TAC (and sham) surgeries were performed in SCOT-Heart-KO and αMHC-Cre control mice, and echocardiographic assessments were performed following 4 wk and 8 wk TAC. Myocardial abundance of SCOT did not significantly change in control animals at 4 wk or 8 wk following TAC surgery (Supplemental Figure 1). Moreover, serum ketone body concentrations did not differ between SCOT-Heart-KO and αMHC-Cre mice after 4 wk TAC, nor did they increase from their respective baseline values; however, serum glucose concentration was modestly elevated after 4 wk TAC in SCOT-Heart-KO mice (Supplemental Table 2). While TAC-induced increases in left ventricular mass were comparable between SCOT-Heart-KO mice and αMHC-Cre control mice at both time points (Figure 3A), mean pressure gradient

 

across the aortic arch was decreased after 8 wk TAC in SCOT-Heart-KO mice, suggesting decreased contractility and abnormal emptying of the left ventricle (Figure 3B). Furthermore, while αMHC-Cre mice maintained preserved systolic function with increased myocardial wall thickness relative to LV chamber size, SCOT-Heart-KO mice exhibited left ventricular dilation with increased end diastolic volume (2.9 ± 0.4 μL/mm tibia length and 5.3 ± 1.0 μL/mm tibia length, respectively; $p = 0.04$; $n = 7$–10/group) and decreased relative wall thickness (Figure 3C, D). In addition, systolic function was markedly decreased in hearts of pressure-overloaded SCOT-Heart-KO mice (ejection fractions of 35.0 ± 7.0%, *versus* 54.9 ± 6.0% in αMHC-Cre control mice; $p = 0.03$; $n = 7$–10/group) (Figure 3D). No statistically significant differences in cardiac output or evidence of worsened pulmonary edema were detected in the SCOT-Heart-KO mice after 8 wk TAC (Supplemental Table 3). Light microscopic analysis of hearts post-TAC revealed no differences in inflammatory infiltrate at either time point (Figure 3E), or in extent of collagen deposition (data not shown). To determine if the accelerated pressure overload-induced ventricular remodeling phenotype could be linked to ultrastructural abnormalities, transmission electron micrographs from SCOT-Heart-KO and αMHC-Cre hearts were compared. Mitochondrial number, organization, and ultrastructural integrity were normal in sham-operated SCOT-Heart-KO mice (Figure 4A–F). Conversely, extensive myofibrilar disarray and Z-line thickening were observed after 4 wk TAC, uniquely within cardiomyocytes from SCOT-Heart-KO mice (Figure 4H, K). High power images revealed no overt differences in mitochondrial ultrastructure relative to αMHC-Cre control mice (Figure 4I, L). Lower power electron micrographs suggest a modest increase in mitochondrial number, with more disordered packing, among myofibrils of SCOT-Heart-KO cardiomyocytes following 4 wk TAC (Figure 4G, J). Quantification of mitochondrial genome copy number indicated a trend towards increased mitochondrial number in hearts of SCOT-Heart-KO mice following 4 wk TAC (Figure 5A, B). Additionally, increased myocardial abundance of the mRNA encoding mitochondrial transcription factor A (TFAM, a mitochondrial transcription factor that coordinates mitochondrial genome replication) was observed in hearts of SCOT-Heart-KO mice following 4 wk TAC (Figure 5C). While phosphorylation of the energy sensor AMPK was normal at baseline and following 4 wk TAC in hearts of SCOT-Heart-KO mice, after 8 wk TAC relative abundance of phosphorylated AMPK was moderately increased in extracts from (Supplemental Figure 2), suggesting delayed energy deficit that was not primarily caused by the absence of ketone body oxidation.

The ultrastructural abnormalities observed following 4 wk TAC in myocardium of SCOT-Heart-KO mice that preceded hemodynamic or structural abnormalities led us to quantify mitochondrial bioenergetics at baseline and following 4 wk TAC. To determine if the modest increase in mitochondrial number may be a compensatory mechanism for abnormal mitochondrial respiratory function, respiration was quantified in mitochondria isolated from hearts of 4 wk sham-operated and post-TAC mice. Substrates palmitoyl-L-carnitine/malate (PLC-M donate electrons to Complexes I and II of the electron transport chain), and succinate/rotenone (S/R, rotenone is a Complex I inhibitor, allowing electrons from succinate to be delivered selectively to Complex II) were tested in independent runs. Mitochondria isolated from hearts of sham SCOT-Heart-KO mice using either PLC-M or S/R revealed no differences in rates of oxygen consumption at state 2 (basal proton leak), 3 (ADP-stimulated), or 4 ($F_1F_0$ ATP-synthase

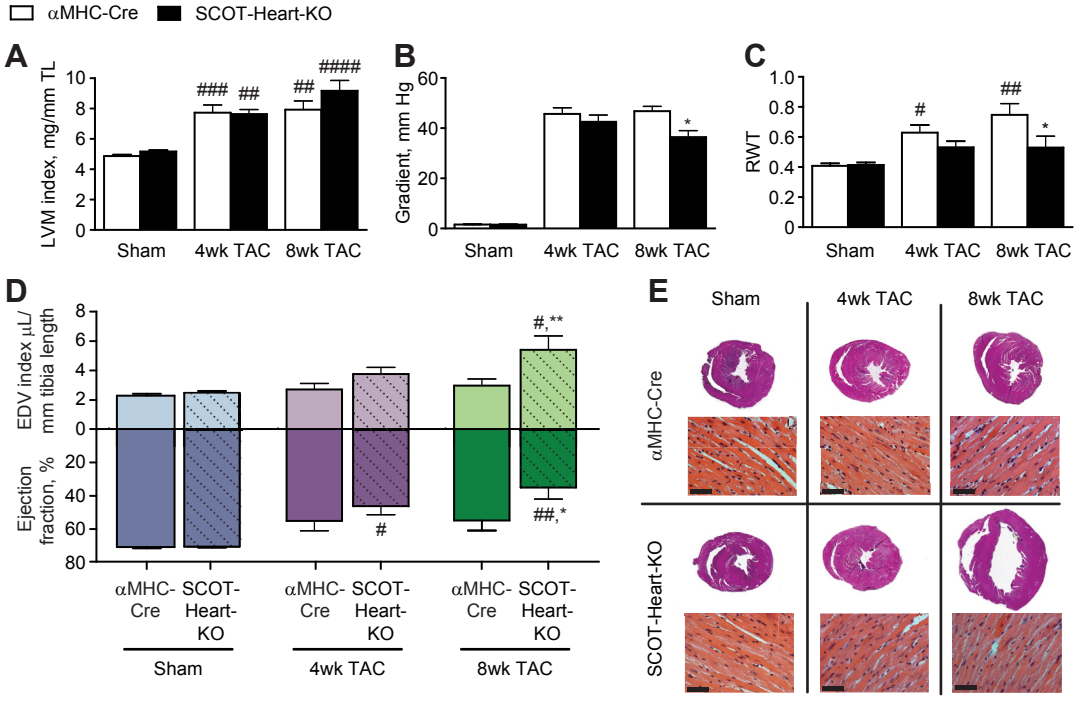


**Figure 3:** SCOT deficiency is associated with worsened pathological remodeling following pressure overload surgery. SCOT-Heart-KO mice and αMHC-Cre controls underwent transverse aortic constriction (TAC) surgery to promote pressure overload-induced pathological remodeling and were analyzed following either 4 wk or 8 wk TAC. (A) Left ventricular mass (LVM) index, mg LV/mm tibia length; (B) Mean pressure gradient across the aortic arch, mmHg; (C) LV relative wall thickness (RWT); and (D) end diastolic volume (EDV) index, mL/mm tibia length, and ejection fraction, %, were all assessed by echocardiography. $n = 5$–10 mice/group. $^{*}p \leq 0.05$, $^{**}p \leq 0.01$ compared to αMHC-Cre mice at same time point; $^{\#}p \leq 0.05$, $^{\#\#}p \leq 0.01$, $^{\#\#\#}p \leq 0.001$, $^{\#\#\#\#}p \leq 0.0001$ compared to baseline time point by 2-way ANOVA with Bonferroni post hoc analysis (E) Representative H&E stained heart cross sections and higher power images. Scale bars are 50 μM.

 

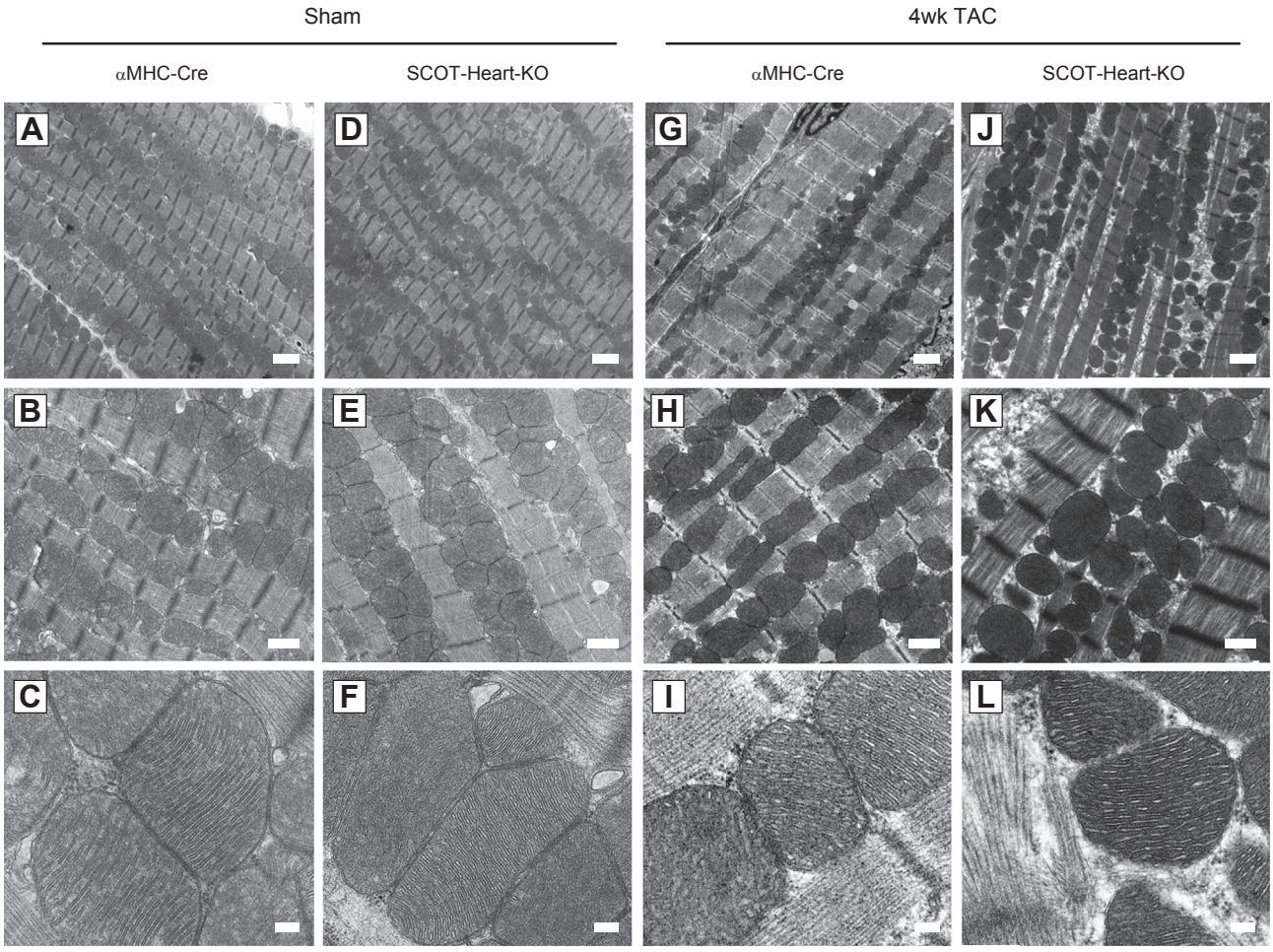


**Figure 4:** Pressure overload-induced ultrastructural abnormalities SCOT-Heart-KO mice. (A, B, D, E) Lower power transmission electron microgrpahs reveal normal cardiac muscle structure in sham operated SCOT-Heart-KO mice. (C, F) High power images show no differences in mitochondrial ultrastructure between genotypes. (G, H, J, K) Following 4 wk TAC, the structural integrity of the myocardium appears compromised in SCOT-Heart-KO mice with evident breakdown of the myofibrils as well as thickening of the Z-lines. (I, L) Despite myofibrilar disarray, mitochondrial ultrastructure appears to be preserved in SCOT-Heart-KO mice. Scale bars are 2 μm (panels A, D, G, J), 1 μM (B, E, H, K), and 200 nm (C, F, I, L). $n = 2$ mice/group.

inhibited) or during uncoupled respiration (provoked by addition of the ionophore FCCP) compared with mitochondria prepared from αMHC-Cre control mice (Figure 5D, E). Furthermore, while S/R-dependent state 2 respiration was decreased for both SCOT-Heart-KO and αMHC-Cre control mitochondria following 4 wk TAC relative to their sham counterparts, PLC-M-dependent state 2 respiration was relatively increased in mitochondria isolated from 4 wk TAC hearts of SCOT-Heart-KO mice, compared with mitochondria prepared from hearts of 4 wk TAC αMHC-Cre control mice. Comparing mitochondria isolated from hearts of sham animals to 4 wk TAC hearts, PLC-M and S/R-dependent state 3 respiration was decreased in both genotypes, reflecting a decrease in ATP synthesis following pressure overload as demonstrated previously in Ref. [46,47], but no differences in state 3 respiration were observed in mitochondria from SCOT-Heart-KO mice. Furthermore, no differences in myocardial protein abundance of the subunits of the electron transport chain including ATP5A (a subunit of the ATPase F1 catalytic core), between hearts of SCOT-Heart-KO and αMHC-Cre mice following either 4 wk or 8 wk TAC (Supplemental Figure 3) were observed. Finally, no differences in $NAD^+$, NADH, NADt or the $NAD^+$/NADH ratio were observed in myocardial extracts from SCOT-Heart-KO mice from the sham or 4 wk TAC conditions (Figure 5F, G). Taken together, these results indicate that despite pressure overload-induced abnormalities of myocyte ultrastructure and mitochondrial packing, SCOT-Heart-KO mice exhibit no overt signs of impaired mitochondrial respiration or cellular redox potential.

### 3.4. Diminished myocardial protein acetylation and increased myocardial ROS in pressure overloaded remodeling hearts of SCOT-Heart-KO mice

Loss of the ability to transfer CoA from succinate to AcAc eliminates one cellular source of acetyl-CoA, which not only serves as a substrate for terminal oxidation in the TCA cycle, but also as a chemical substrate for post-translational modification of numerous structural proteins and enzymes in mitochondrial and cytoplasmic compartments, significantly influencing their downstream functions [48]. To determine if loss of SCOT in cardiomyocytes is associated with a change in abundance of acetylated lysine residues among myocardial proteins we performed immunoblots of myocardial and isolated mitochondrial isolates using an antibody raised against acetylated lysine. At baseline, abundance of acetylated proteins was modestly, but nearly significantly decreased in total myocardial extracts (Figure 6A). Mitochondria isolated from SCOT-Heart-KO and αMHC-Cre control hearts at baseline did reveal

 

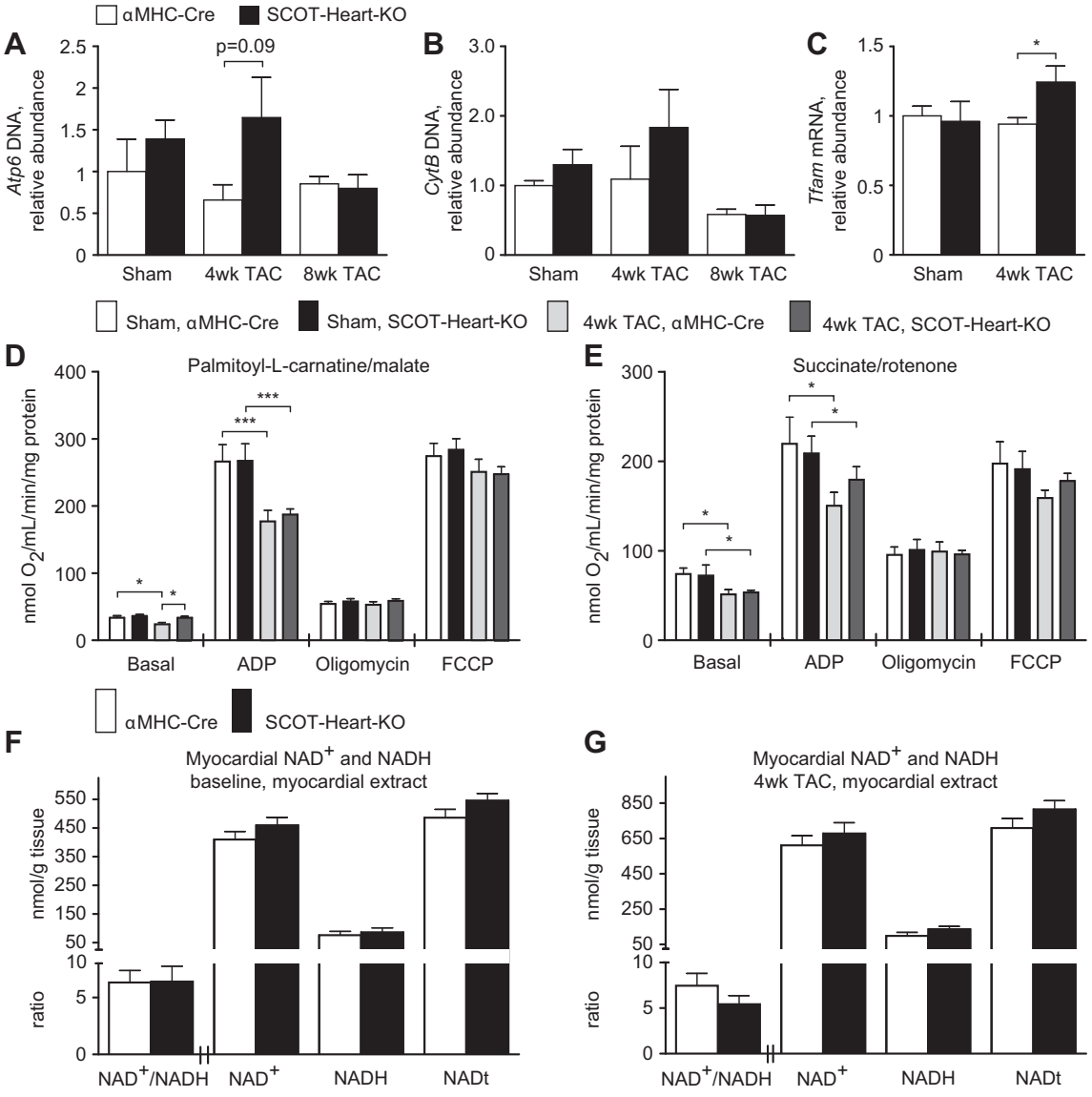


**Figure 5:** Relative genome content and respiration studies of cardiac mitochondria. (A, B) Quantification of mitochondrial genome copy number (relative abundance) by qPCR using purified heart gDNA from SCOT-Heart-KO and αMHC-Cre mice at baseline, or after 4 wk or 8 wk TAC. Data are presented as means ± SEM; $n = 4–5$/group, $^*p \leq 0.05$ by 1-way ANOVA with Tukey's post hoc analysis. (C) Increased myocardial expression of mitochondrial transcription factor A (*Tfam*). (D, E) Respiration rates in the basal leak condition (state 2), ADP-stimulated condition (state 3), $F_1F_0$-ATPase independent condition (state 4, oligomycin), and uncoupled condition (FCCP) in mitochondria isolated from left ventricles of SCOT-Heart-KO and αMHC-Cre mice using palmitoyl-L-carnitine and malate or succinate and rotenone as substrates at (D) baseline or (E) following 4 wk TAC. Data are presented as means ± SEM; $n = 4–7$ mice/group, $^*p \leq 0.05$, $^{***}p \leq 0.001$ by 2-way ANOVA with Bonferroni post hoc analysis. (F, G) No differences in $NAD^+$, NADH, NADt or $NAD^+$/NADH ratios were detected when comparing whole myocardial lysates of SCOT-Heart-KO and αMHC-Cre control mice at (F) baseline or (G) after 4 wk TAC. $n = 5–7$ mice/group.

significant diminution in content of acetylated lysine in knockout mitochondria (Figure 6B). Moreover, total myocardial extracts prepared following 4 wk TAC also demonstrated a significant reduction in the quantity of acetylated lysine residues in hearts isolated from SCOT-Heart-KO mice (Figure 6C).

Lysine residues are modified by numerous post-translational modifications in addition to acetylation, and individual lysine residues may be acetylated or succinylated [49]. Because SCOT transfers CoA between succinate and AcAc, loss of SCOT could theoretically alter the pools of succinate/succinyl-CoA available for numerous downstream reactions, including succinylation of lysine residues. To determine myocardial succinate concentrations in SCOT-Heart-KO mice, we quantified its pool sizes by NMR in *ex vivo* perfused hearts, and observed that total myocardial succinate content was commensurate with that of control mice (Supplemental Figure 4A, B). However, when lactate was omitted from the perfusion buffer the myocardial succinate pool size was significantly diminished in SCOT-Heart-KO mice (Supplemental Figure 4C), consistent with reduced concentrations of other metabolites under this perfusion condition (see Figure 2E, F). A modest trend towards diminished abundance of succinylated lysine residues was also observed in unperfused myocardial extracts prepared following 4 wk TAC (Supplemental Figure 4D). Taken together, loss of SCOT may yield modest context-selective diminution of the succinate pool size, but decreased lysine acetylation in SCOT-Heart-KO myocardium is unlikely to be attributable to increased lysine succinylation.

 

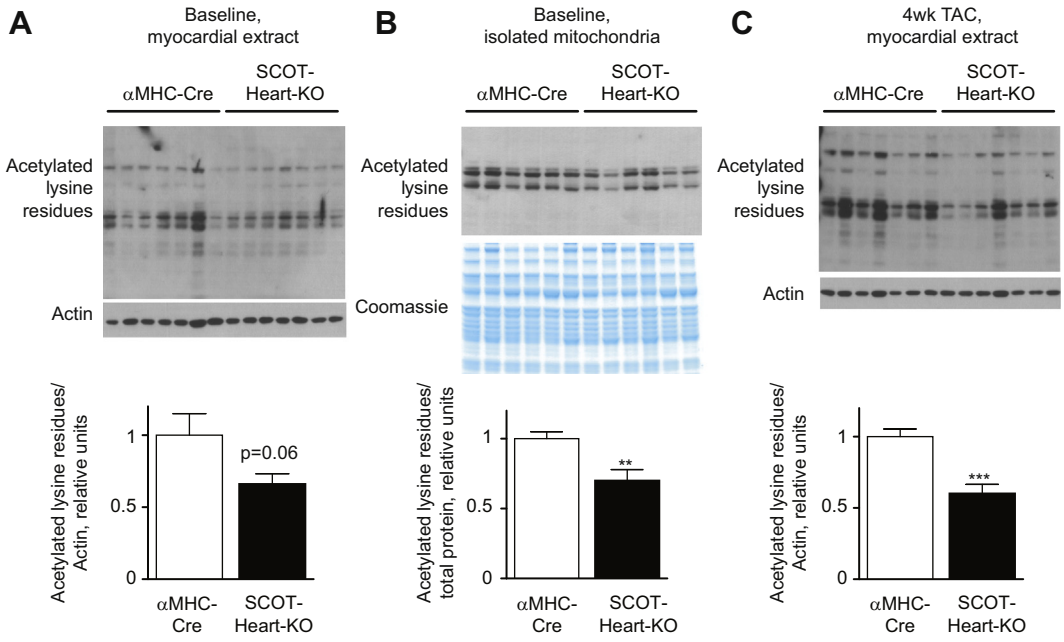


**Figure 6:** Decreased acetylation of lysine residues in myocardial proteins of SCOT-Heart-KO mice. Decreased acetylation of lysine residues is evident at baseline in both (A) whole myocardial and (B) isolated mitochondrial protein extracts as well as (C) after 4 wk TAC in whole myocardial extracts. $n = 5-7$ mice/group, $^{*}p \leq 0.05$, $^{**}p \leq 0.01$, $^{***}p \leq 0.001$ by Student's *t* test.

Deacetylation of specific electron transport chain subunits, including NDUFS1 of complex I and the Rieseke subunit of cytochrome bc1, have been shown to attenuate ROS generation in the setting of ischemia/reperfusion injury [50]. Moreover, procession of ketone bodies through the SCOT enzyme toward terminal oxidation attenuates ROS production from oxidation of fatty acids [21—23]. Therefore, we hypothesized that loss of SCOT activity would be associated with increased mitochondrial ROS production, augmenting injury and remodeling responses, particularly in the setting of pressure overload-induced remodeling. Mitochondrial oxidative metabolism *via* the electron transport chain is the major source of ROS within cardiomyocytes [23,51]. To determine if the SCOT deficiency and increased reliance on oxidation of fatty acids was associated with increased mitochondrial ROS production, mitochondria isolated from hearts of SCOT-Heart-KO and αMHC-Cre mice were incubated with 10 mM succinate, succinate plus 1 mM D-βOHB, or succinate plus 1 mM AcAc, and $H_2O_2$ emission was quantified as a reporter of mitochondrial superoxide production. While no difference in the rates of $H_2O_2$ production between the two genotypes was observed, independent of SCOT genotype, addition of 1 mM AcAc to the substrate buffer significantly diminished rates of $H_2O_2$ production compared to mitochondria incubated with succinate alone, or succinate plus D-βOHB (Figure 7A).

To determine the impact of SCOT deficiency on tissue ROS abundance, superoxide was quantified *in situ* using fluorescent probes. In fresh frozen myocardial sections prepared from sham-operated animals, myocardial superoxide content was normal, while fresh frozen myocardial sections from 4 wk TAC hearts revealed significantly increased total superoxide accumulation, and a trend towards increased mitochondrial/nuclear superoxide accumulation was evident in myocardial sections prepared from SCOT-Heart-KO mice (Figure 7B). Increased ROS levels may lead to oxidative protein damage including protein carbonylation, and the oxidation of protein residues can be detected and quantified *via* Western blotting following a reaction by 2,4-dinitrophenylhydrazine (DNPH) [52]. While there were no differences in the quantity of carbonylated myocardial proteins between sham-operated SCOT-Heart-KO and αMHC-Cre mice (raw data not shown, Figure 7C), following 4 wk TAC, pressure-overloaded hearts of SCOT-Heart-KO mice exhibited a two-fold increase in the quantity of carbonylated myocardial proteins, supporting a role for ketone body oxidation in the diminution of ROS in the setting of pressure overload injury (Figure 7C). These data indicate that the absolute deficiency of myocardial ketone body oxidation is deleterious during pressure overload-induced remodeling possibly due, at least in part, to increased oxidative stress in the myocardium.

## 4. DISCUSSION

Normal heart muscle is relatively omnivorous, flexibly converting the energy stored in a diverse menu of substrates to high energy phosphates. Whereas myocardial glucose and fat utilization have been extensively studied for their role in modulating cardiac function in pathological states [4,5,53], the importance of ketone body metabolism under both physiological and pathological conditions has not been carefully scrutinized. Adherence of wild type mice to high fat, very low carbohydrate ketogenic diets is well-tolerated and causes only subtle hemodynamic effects. Using mice that exhibit loss of SCOT specifically in cardiac myocytes, we determined the role of myocardial ketone body metabolism under baseline conditions, and conditions known to increase myocardial fat and ketone metabolism including starvation and maintenance on a ketogenic diet. Hearts lacking the ability to oxidize ketone bodies rely more heavily on fatty acid oxidation when both fat and ketones are available as substrates. However, few differences were found between SCOT-Heart-KO and control mice during periods of increased reliance on fat and increased myocardial ketone delivery, which indicates that the ability of the SCOT-Heart-KO mice to convert the energy stored within fatty acids to high energy phosphates protects from the loss of ketone body utilization, and that ketone body oxidation is not required in hemodynamically normal

 

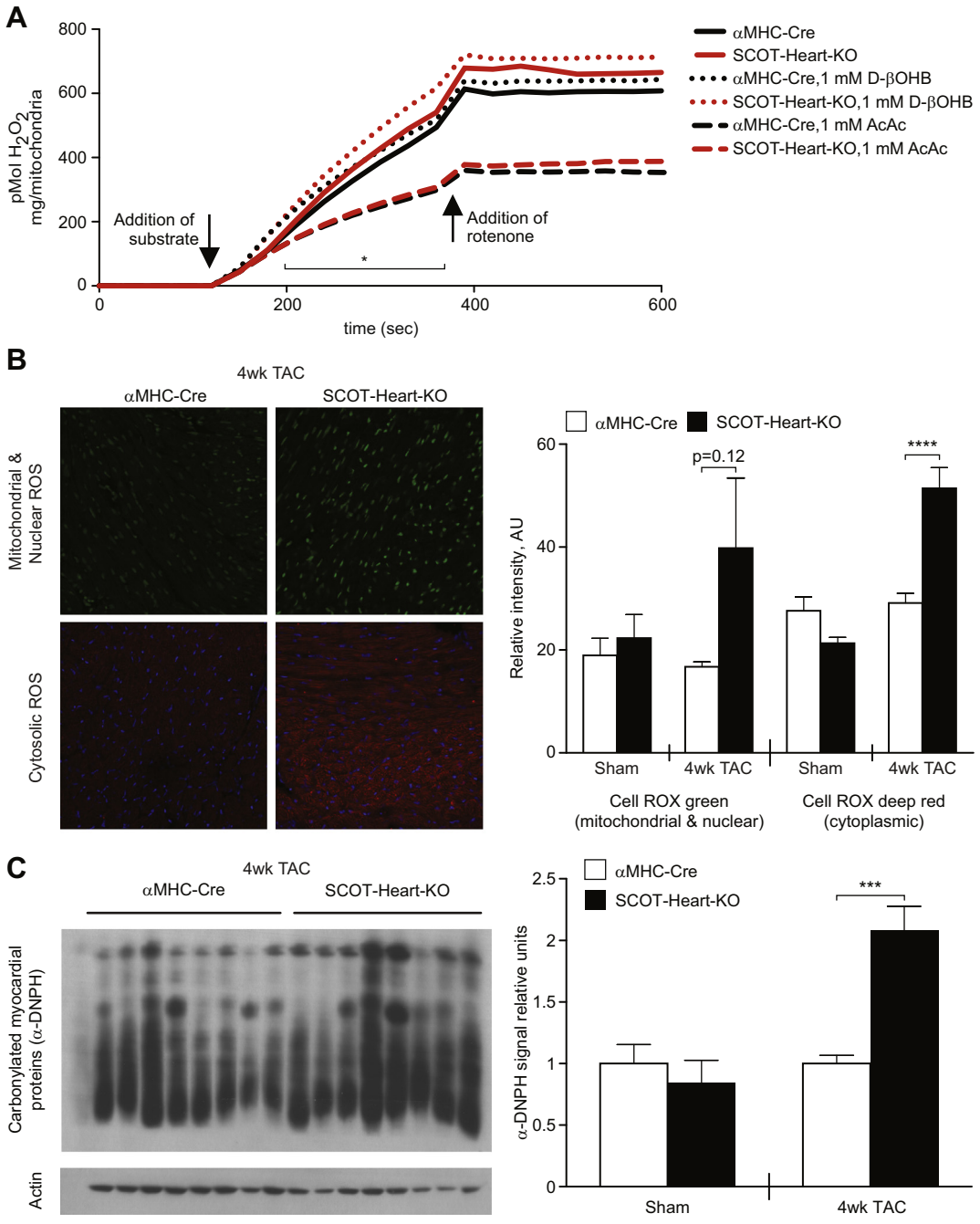


**Figure 7:** Pressure-overload-induced signatures of increased oxidative stress in SCOT-Heart-KO mice. (A) $H_2O_2$ emission was measured in isolated mitochondria following the addition of metabolic substrate (i) succinate, (ii) succinate plus D-βOHB, or (iii) succinate plus acetoacetate (AcAc); rotenone was added to eliminate further $H_2O_2$ emission. *$p = 0.02$ and $p = 0.04$ for rates of $H_2O_2$ emission following the addition of succinate plus AcAc in SCOT-Heart-KO and αMHC-Cre mitochondria, respectively, when compared with the rates of $H_2O_2$ emission following the addition of succinate alone, $n = 7$ mice/group. (B) Tissue superoxide content was quantified *in situ* using fluorogenic probes CellROX® Green, detecting mitochondrial and nuclear ROS and CellROX® Deep Red reagent detecting cytosolic ROS. Relative intensity was quantified using ImageJ. Sham operated images not shown. (C) Protein oxidation was quantified in whole myocardial lysates of SCOT-Heart-KO and αMHC-Cre mice *via* Western blotting following a reaction by 2,4-dinitrophenylhydrazine (DNPH). Sham operated blot not shown. $n = 3–7$ mice/group. ***$p \leq 0.001$, ****$p \leq 0.0001$ by 2-way ANOVA with Bonferroni post hoc analysis.

hearts. To determine how SCOT-Heart-KO mice adapt to pathological states in which reliance on fatty acid oxidation is normally shifted toward glucose metabolism, we employed experimental conditions that diminish myocardial fatty acid oxidation, including the systemic inflammatory response (LPS) and myocardial pressure overload (TAC). In particular, while control mice exhibit compensated remodeling with concentric LV hypertrophy and preserved ejection fraction in response to pressure overload, SCOT-Heart-KO mice develop adverse ventricular remodeling with LV dilation and reduced ejection fraction. Despite systolic dysfunction, stroke volume and cardiac output were normal in these experiments, due to the increased left ventricular end diastolic volume. Nonetheless, these studies demonstrate that complete

 

elimination of ketone bodies as an energy source drives hearts toward a more adverse remodeling course of LV dilation [54].

Numerous studies have explored the complex relationship between myocardial substrate utilization and pathological remodeling in the hypertrophied heart — namely an increased reliance on glucose utilization and concomitant reduction of fatty acid oxidative contribution to energy production [55], and increased anaplerosis [56,57] (for a review on myocardial anaplerosis, see Ref. [58]). These metabolic alterations conspire to produce energetic inefficiencies in the hypertrophied and, ultimately, failing heart [45]. Transgenic overexpression of GLUT1 in the murine myocardium increases glucose utilization, attenuates cardiac hypertrophy and maintains myocardial phosphocreatine and ATP levels [59]. Genetically encoded increases in fatty acid oxidation (*via* knockout of mitochondrial acetyl-CoA carboxylase) in hypertrophic remodeling reveals a significant reduction in hypertrophic growth and fibrosis, as well as a reduction in anaplerotic flux, which were associated with improved contractility in the pressure overloaded heart [57]. Our study suggests (i) preservation of fatty acid oxidation in the remodeling heart may be salutary, as long as ketone body oxidation is preserved and (ii) a modest increase in anaplerosis in SCOT-Heart-KO mice at baseline, in the absence of any hemodynamic abnormalities. Thus, the inability to oxidize ketones may predispose the heart to metabolic reprogramming that contributes to worsened remodeling following pressure overload. While our data do not provide evidence that indicates altered abundances of steady state acetyl-CoA pool sizes in the absence of SCOT, future untargeted interrogations of the SCOT-deficient metabolome will reveal how metabolic redundancy supports a compensated response to the absence of ketolytic capacity in physiological states of robust myocardial ketone body delivery.

The induction of pressure overload hypertrophy is associated with increased oxidative stress [24,60,61]. Hearts of SCOT-Heart-KO mice exhibit increased signatures of oxidative stress following 4 wk TAC — prior to the development of structural and hemodynamic abnormalities. Thus, increased oxidative stress could play a causative role in the remodeling course exhibited by the hearts of these mice. ROS cause oxidative modification of myocardial proteins and lipids, and create bioenergetic insufficiency *via* uncoupling [62—66]. The mechanism of ketone bodies and their metabolism to regulate myocardial ROS abundance and oxidative stress is incompletely understood. Ketone bodies may be more energetically favorable substrates than fatty acids, in part through the maintenance of a favorable $NAD^+$/NADH ratio as well as their ability to maintain ubiquinone in the oxidized state, which increases redox span in the electron transport chain and thus diminishes superoxide production and increases energy available for ATP synthesis [22]. Several *in vitro* studies support this theory. For example, equimolar D-βOHB and AcAc attenuates ROS abundance of isolated neurons [67,68]. In our study, AcAc diminished the rate of superoxide production in mitochondria isolated from hearts of both SCOT-Heart-KO and control mice, which suggests that AcAc-mediated suppression of mitochondrial superoxide emission is likely due to a non-oxidative role of AcAc, whose mechanisms could include ROS scavenging by AcAc, or diminished mitochondrial inner membrane potential through non-oxidative mechanisms [23]. Finally, ketone bodies and SCOT activity can potentially influence the balance of ROS production and scavenging from mitochondrial and extra-mitochondrial sources [69].

Our study also demonstrates a correlation between SCOT enzyme activity and protein acetylation, with SCOT-Heart-KO mice exhibiting significant diminutions in acetylated lysine residues at baseline and following 4 wk TAC. Numerous myocardial proteins are regulated by this post-translational modification, including critical mediators of myocardial fatty acid oxidation, the TCA cycle, and the electron transport chain [70,71]. SCOT itself has been identified in a number of screens to identify mitochondrial proteins with numerous acetylation sites [70,72]. Whether acetylation of SCOT impairs or enhances enzyme activity has yet to be determined, however, a study in hypertrophic rat models demonstrates that SCOT is hyperacetylated in these rats relative to non-hypertensive controls [72]. The role of mitochondrial deacetylase SIRT3 as an amplifier of antioxidant defense mechanisms in the remodeling heart underscores the intriguing connection between myocardial protein acetylation and oxidative stress [73,74], and thus the possibility that protein acetylation influences the observed ROS phenotypes in pressure-overloaded hearts of SCOT-Heart-KO mice will be a target of future investigation. Protein acetylation is also a common modification among sarcomeric proteins that mediate contractility [70,75,76], and *in vitro* experiments indicate that increased acetylation of these myosin isoforms correlates with increased actin sliding velocity, suggesting that acetylation of mechanical proteins post-TAC may play an important homeostatic role [76].

In some cell types, increased delivery of the ketone body D-βOHB increases histone acetylation, which ameliorates oxidative stress through an ability to increase transcription of *Foxo3a* and *Mt2 via* inhibition of Class I histone deacetylases [77]. In our study, we demonstrated that despite the absence of SCOT in the myocardium, serum ketone body concentrations do not differ compared with control mice. Although myocardium is the highest ketone body consumer per mass, other ketolytic tissues (*e.g.*, brain, skeletal muscle) could increase ketone body uptake and consumption to modulate circulating ketone body concentrations. Nonetheless, no alterations in *Foxo3a* or *Mt2* mRNA myocardial abundances were detected in hearts of SCOT-Heart-KO mice at baseline or following 4 wk TAC (data not shown).

## 5. CONCLUSIONS

These are the first studies to systematically interrogate myocardial responses of hearts unable to oxidize ketone bodies, during ketotic states and non-ketotic pathological states. Our findings are consistent with the notion that myocardial ketone body metabolism integrates the response to myocardial injury, in part through the maintenance of protein acetylation and ROS homeostasis. However, it is also important to note that the normal heart may counter-regulate against 'excessive' metabolism of ketone bodies when increased delivery is sustained [33]. Therefore, the clinical applicability of these studies still remains incompletely defined, and targeted studies must quantify the oxidation of ketone bodies by the human remodeling heart to decipher whether an optimal window of myocardial ketone metabolism could confer myocardial protection from oxidative stress and adverse signaling, while preventing adverse metabolic consequences of 'excessive' ketone body oxidation, *e.g.*, impaired metabolic flexibility. Because systemic ketone body metabolism, and thus myocardial delivery of ketone bodies, can be dynamically modified through nutritional means, understanding the role of ketone body metabolism in the injured and remodeling heart may hold promising downstream diagnostic and therapeutic implications.

## ACKNOWLEDGMENTS

We thank Lela Pritchett for technical assistance, members of the laboratory, Dan Kelly, Doug Lewandowski, Heinrich Taegtmeyer, and Christine Des Rosiers for helpful discussions, and Laura Kyro for assistance with graphics. This work was supported by the National Institutes of Health, DK-091538 (to P.A. Crawford), the

 

Diabetes Research Center (DK-020579), the Nutrition and Obesity Research Center (DK-056341), the Digestive Disease Research Core Center (DK-052574), Training Grant HL-007275 (for R.C. Schugar), the Children's Discovery Institute through St. Louis Children's Hospital Foundation (to P.A. Crawford), and the David and Deborah Winston Fellowship in Diabetic Cardiovascular Research (to R.C. Schugar).

## CONFLICT OF INTEREST

None declared.

## APPENDIX A. SUPPLEMENTARY DATA

Supplementary data related to this article can be found at http://dx.doi.org/10.1016/j.molmet.2014.07.010.

## REFERENCES

[1] Abel, E.D., Doenst, T., 2011. Mitochondrial adaptations to physiological versus pathological cardiac hypertrophy. Cardiovascular Research 90:234–242.
[2] Ashrafian, H., Frenneaux, M.P., Opie, L.H., 2007. Metabolic mechanisms in heart failure. Circulation 116:434–448.
[3] Boudina, S., Abel, E.D., 2010. Diabetic cardiomyopathy, causes and effects. Reviews in Endocrine and Metabolic Disorders 11:31–39.
[4] Kolwicz Jr., S.C., Tian, R., 2011. Glucose metabolism and cardiac hypertrophy. Cardiovascular Research 90:194–201.
[5] Lopaschuk, G.D., Ussher, J.R., Folmes, C.D., Jaswal, J.S., Stanley, W.C., 2010. Myocardial fatty acid metabolism in health and disease. Physiological Reviews 90:207–258.
[6] Jaswal, J.S., Keung, W., Wang, W., Ussher, J.R., Lopaschuk, G.D., 2011. Targeting fatty acid and carbohydrate oxidation – a novel therapeutic intervention in the ischemic and failing heart. Biochimica Biophysica Acta 1813:1333–1350.
[7] Fillmore, N., Lopaschuk, G.D., 2013. Targeting mitochondrial oxidative metabolism as an approach to treat heart failure. Biochimica Biophysica Acta 1833:857–865.
[8] Lommi, J., Kupari, M., Koskinen, P., Naveri, H., Leinonen, H., Pulkki, K., et al., 1996. Blood ketone bodies in congestive heart failure. Journal of the American College of Cardiology 28:665–672.
[9] Lommi, J., Koskinen, P., Naveri, H., Harkonen, M., Kupari, M., 1997. Heart failure ketosis. Journal of Internal Medicine 242:231–238.
[10] Du, Z., Shen, A., Huang, Y., Su, L., Lai, W., Wang, P., et al., 2014. 1H-NMR-based metabolic analysis of human serum reveals novel markers of myocardial energy expenditure in heart failure patients. PLoS ONE 9:e88102.
[11] Cotter, D.G., Schugar, R.C., Crawford, P.A., 2013. Ketone body metabolism and cardiovascular disease. American Journal of Physiology Heart and Circulatory Physiology 304:1060–1076.
[12] Fukao, T., Mitchell, G., Sass, J.O., Hori, T., Orii, K., Aoyama, Y., 2014 Jul. Ketone body metabolism and its defects. Journal of Inherited Metabolic Disease 37(4):541–551 [Epub ahead of print. PMID: 24706027].
[13] Cotter, D.G., d'Avignon, D.A., Wentz, A.E., Weber, M.L., Crawford, P.A., 2011. Obligate role for ketone body oxidation in neonatal metabolic homeostasis. Journal of Biological Chemistry 286:6902–6910.
[14] Bing, R.J., 1955. The metabolism of the heart. Harvey Lectures 50:27–70.
[15] Garland, P.B., Newsholme, E.A., Randle, P.J., 1962. Effect of fatty acids, ketone bodies, diabetes and starvation on pyruvate metabolism in rat heart and diaphragm muscle. Nature 195:381–383.
[16] Jeffrey, F.M., Diczku, V., Sherry, A.D., Malloy, C.R., 1995. Substrate selection in the isolated working rat heart: effects of reperfusion, afterload, and concentration. Basic Research in Cardiology 90:388–396.
[17] Tardif, A., Julien, N., Pelletier, A., Thibault, G., Srivastava, A.K., Chiasson, J.L., et al., 2001. Chronic exposure to beta-hydroxybutyrate impairs insulin action in primary cultures of adult cardiomyocytes. American Journal of Physiology. Endocrinology and Metabolism 281:E1205–E1212.
[18] Hasselbaink, D.M., Glatz, J.F., Luiken, J.J., Roemen, T.H., Van der Vusse, G.J., 2003. Ketone bodies disturb fatty acid handling in isolated cardiomyocytes derived from control and diabetic rats. Biochemical Journal 371:753–760.
[19] Crawford, P.A., Crowley, J.R., Sambandam, N., Muegge, B.D., Costello, E.K., Hamady, M., et al., 2009. Regulation of myocardial ketone body metabolism by the gut microbiota during nutrient deprivation. Proceedings of the National Academy of Sciences of the United States of America 106:11276–11281.
[20] Kashiwaya, Y., Sato, K., Tsuchiya, N., Thomas, S., Fell, D.A., Veech, R.L., et al., 1994. Control of glucose utilization in working perfused rat heart. Journal of Biological Chemistry 269:25502–25514.
[21] Sato, K., Kashiwaya, Y., Keon, C.A., Tsuchiya, N., King, M.T., Radda, G.K., et al., 1995. Insulin, ketone bodies, and mitochondrial energy transduction. FASEB Journal 9:651–658.
[22] Veech, R.L., 2004. The therapeutic implications of ketone bodies: the effects of ketone bodies in pathological conditions: ketosis, ketogenic diet, redox states, insulin resistance, and mitochondrial metabolism. Prostaglandins Leukotrienes and Essential Fatty Acids 70:309–319.
[23] Murphy, M.P., 2009. How mitochondria produce reactive oxygen species. Biochemical Journal 417:1–13.
[24] Dai, D.F., Hsieh, E.J., Liu, Y., Chen, T., Beyer, R.P., Chin, M.T., et al., 2012. Mitochondrial proteome remodelling in pressure overload-induced heart failure: the role of mitochondrial oxidative stress. Cardiovascular Research 93:79–88.
[25] Fukao, T., Sakurai, S., Rolland, M.O., Zabot, M.T., Schulze, A., Yamada, K., et al., 2006. A 6-bp deletion at the splice donor site of the first intron resulted in aberrant splicing using a cryptic splice site within exon 1 in a patient with succinyl-CoA: 3-Ketoacid CoA transferase (SCOT) deficiency. Molecular Genetics and Metabolism 89:280–282.
[26] Longo, N., Fukao, T., Singh, R., Pasquali, M., Barrios, R.G., Kondo, N., et al., 2004. Succinyl-CoA:3-ketoacid transferase (SCOT) deficiency in a new patient homozygous for an R217X mutation. Journal of Inherited Metabolic Disease 27:691–692.
[27] Tildon, J.T., Cornblath, M., 1972. Succinyl-CoA: 3-ketoacid CoA-transferase deficiency. A cause for ketoacidosis in infancy. Journal of Clinical Investigation 51:493–498.
[28] Saudubray, J.M., Specola, N., Middleton, B., Lombes, A., Bonnefont, J.P., Jakobs, C., et al., 1987. Hyperketotic states due to inherited defects of ketolysis. Enzyme 38:80–90.
[29] Janardhan, A., Chen, J., Crawford, P.A., 2011. Altered systemic ketone body metabolism in advanced heart failure. Texas Heart Institute Journal 38:533–538.
[30] Rudolph, W., Schinz, A., 1973. Studies on myocardial blood flow, oxygen consumption, and myocardial metabolism in patients with cardiomyopathy. Recent Advances in Studies on Cardiac Structure and Metabolism 2:739–749.
[31] Cotter, D.G., Schugar, R.C., Wentz, A.E., d'Avignon, D.A., Crawford, P.A., 2013. Successful adaptation to ketosis by mice with tissue-specific deficiency of ketone body oxidation. American Journal of Physiology. Endocrinology and Metabolism 304:363–374.
[32] Schugar, R.C., Crawford, P.A., 2012. Low-carbohydrate ketogenic diets, glucose homeostasis, and nonalcoholic fatty liver disease. Current Opinion in Clinical Nutrition and Metabolic Care 15:374–380.
[33] Wentz, A.E., d'Avignon, D.A., Weber, M.L., Cotter, D.G., Doherty, J.M., Kerns, R., et al., 2010. Adaptation of myocardial substrate metabolism to a ketogenic nutrient environment. Journal of Biological Chemistry 285:24447–24456.
[34] Cotter, D., Ercal, B., d'Avignon, D., Dietzen, D., Crawford, P., 2013. Impact of peripheral ketolytic deficiency on hepatic ketogenesis and gluconeogenesis

 

during the transition to birth. Journal of Biological Chemistry 288:19739–19749.

[35] Huss, J.M., Imahashi, K., Dufour, C.R., Weinheimer, C.J., Courtois, M., Kovacs, A., et al., 2007. The nuclear receptor ERRalpha is required for the bioenergetic and functional adaptation to cardiac pressure overload. Cell Metabolism 6:25–37.

[36] Rogers, J., Tamirisa, P., Kovacs, A., Weinheimer, C., Courtois, M., Blumer, K., et al., 1999. RGS4 causes increased mortality and reduced cardiac hypertrophy in response to pressure overload. Journal of Clinical Investigation 104:567–576.

[37] Lehman, J.J., Boudina, S., Banke, N.H., Sambandam, N., Han, X., Young, D.M., et al., 2008. The transcriptional coactivator PGC-1alpha is essential for maximal and efficient cardiac mitochondrial fatty acid oxidation and lipid homeostasis. American Journal of Physiology Heart and Circulatory Physiology 295:H185–H196.

[38] Kimura, I.I.D., Maeda, T., Hara, T., Ichimura, A., Miyauchi, S., Kobayashi, M., et al., 2011. Short-chain fatty acids and ketones directly regulate sympathetic nervous system via G protein-coupled receptor 41 (GPR41). Proceedings of National Academy of Sciences 108:8030–8035.

[39] Stowe, K.A., Burgess, S.C., Merritt, M., Sherry, A.D., Malloy, C.R., 2006. Storage and oxidation of long-chain fatty acids in the C57/BL6 mouse heart as measured by NMR spectroscopy. FEBS Letters 580:4282–4287.

[40] Gaussin, V., Van de Putte, T., Mishina, Y., Hanks, M.C., Zwijsen, A., Huylebroeck, D., et al., 2002. Endocardial cushion and myocardial defects after cardiac myocyte-specific conditional deletion of the bone morphogenetic protein receptor ALK3. Proceedings of the National Academy of Sciences of the United States of America 99:2878–2883.

[41] Jones, J.G., Hansen, J., Sherry, A.D., Malloy, C.R., Victor, R.G., 1997. Determination of acetyl-CoA enrichment in rat heart and skeletal muscle by 1H nuclear magnetic resonance analysis of glutamate in tissue extracts. Analytical Biochemistry 249:201–206.

[42] Befroy, D.E., Perry, R.J., Jain, N., Dufour, S., Cline, G.W., Trimmer, J.K., et al., 2014 Jan. Direct assessment of hepatic mitochondrial oxidative and anaplerotic fluxes in humans using dynamic 13C magnetic resonance spectroscopy. Nature Medicine 20(1):98–102.

[43] Suzuki, J., Shen, W.J., Nelson, B.D., Selwood, S.P., Murphy Jr., G.M., Kanehara, H., et al., 2002. Cardiac gene expression profile and lipid accumulation in response to starvation. American Journal of Physiology. Endocrinology and Metabolism 283:E94–E102.

[44] Schilling, J., Lai, L., Sambandam, N., Dey, C.E., Leone, T.C., Kelly, D.P., 2011 Jul. Toll-like receptor-mediated inflammatory signaling reprograms cardiac energy metabolism by repressing peroxisome proliferator-activated receptor gamma coactivator-1 signaling. Circulation Heart Failure 4(4):474–482.

[45] Neubauer, S., 2007. The failing heart — an engine out of fuel. New England Journal of Medicine 356:1140–1151.

[46] Pereira, R.O., Wende, A.R., Crum, A., Hunter, D., Olsen, C.D., Rawlings, T., et al., 2014 Aug 28. Maintaining PGC-1alpha expression following pressure overload-induced cardiac hypertrophy preserves angiogenesis but not contractile or mitochondrial function. FASEB Journal 28(8):3691–3702.

[47] Gupta, A., Chacko, V.P., Schar, M., Akki, A., Weiss, R.G., Jan 2011. Impaired ATP kinetics in failing in vivo mouse heart. Circulation Cardiovascular Imaging 4(1):42–50.

[48] Spange, S., Wagner, T., Heinzel, T., Kramer, O.H., 2009. Acetylation of non-histone proteins modulates cellular signalling at multiple levels. International Journal of Biochemistry & Cell Biology 41:185–198.

[49] Weinert, B.T., Scholz, C., Wagner, S.A., Iesmantavicius, V., Su, D., Daniel, J.A., et al., 2013. Lysine succinylation is a frequently occurring modification in prokaryotes and eukaryotes and extensively overlaps with acetylation. Cell Reports 4:842–851.

[50] Shinmura, K., Tamaki, K., Sano, M., Nakashima-Kamimura, N., Wolf, A.M., Amo, T., et al., 2011 Aug 5. Caloric restriction primes mitochondria for ischemic stress by deacetylating specific mitochondrial proteins of the electron transport chain. Circulation Research 109(4):396–406.

[51] Turrens, J.F., 2003. Mitochondrial formation of reactive oxygen species. The Journal of Physiology 552:335–344.

[52] Dalle-Donne, I., Aldini, G., Carini, M., Colombo, R., Rossi, R., Milzani, A., 2006. Protein carbonylation, cellular dysfunction, and disease progression. Journal of Cellular and Molecular Medicine 10:389–406.

[53] Drosatos, K., Schulze, P.C., 2013 Jun. Cardiac lipotoxicity: molecular pathways and therapeutic implications. Current Heart Failure Reports 10(2):109–121.

[54] Mann, D.L., Bogaev, R., Buckberg, G.D., 2010. Cardiac remodelling and myocardial recovery: lost in translation? European Journal of Heart Failure 12:789–796.

[55] Allard, M.F., Schonekess, B.O., Henning, S.L., English, D.R., Lopaschuk, G.D., 1994. Contribution of oxidative metabolism and glycolysis to ATP production in hypertrophied hearts. American Journal of Physiology 267:H742–H750.

[56] Pound, K.M., Sorokina, N., Ballal, K., Berkich, D.A., Fasano, M., Lanoue, K.F., et al., 2009. Substrate-enzyme competition attenuates upregulated anaplerotic flux through malic enzyme in hypertrophied rat heart and restores triacylglyceride content: attenuating upregulated anaplerosis in hypertrophy. Circulation Research 104:805–812.

[57] Kolwicz Jr., S.C., Olson, D.P., Marney, L.C., Garcia-Menendez, L., Synovec, R.E., Tian, R., 2012. Cardiac-specific deletion of acetyl CoA carboxylase 2 prevents metabolic remodeling during pressure-overload hypertrophy. Circulation Research 111:728–738.

[58] Des Rosiers, C., Labarthe, F., Lloyd, S.G., Chatham, J.C., 2011. Cardiac anaplerosis in health and disease: food for thought. Cardiovascular Research 90:210–219.

[59] Liao, R., Jain, M., Cui, L., D'Agostino, J., Aiello, F., Luptak, I., et al., 2002. Cardiac-specific overexpression of GLUT1 prevents the development of heart failure attributable to pressure overload in mice. Circulation 106:2125–2131.

[60] Dai, D.F., Johnson, S.C., Villarin, J.J., Chin, M.T., Nieves-Cintron, M., Chen, T., et al., 2011. Mitochondrial oxidative stress mediates angiotensin II-induced cardiac hypertrophy and Galphaq overexpression-induced heart failure. Circulation Research 108:837–846.

[61] Dai, D.F., Hsieh, E.J., Chen, T., Menendez, L.G., Basisty, N.B., Tsai, L., et al., 2013. Global proteomics and pathway analysis of pressure-overload-induced heart failure and its attenuation by mitochondrial-targeted peptides. Circulation Heart Failure 6:1067–1076.

[62] Echtay, K.S., Roussel, D., St-Pierre, J., Jekabsons, M.B., Cadenas, S., Stuart, J.A., et al., 2002. Superoxide activates mitochondrial uncoupling proteins. Nature 415:96–99.

[63] Turko, I.V., Li, L., Aulak, K.S., Stuehr, D.J., Chang, J.Y., Murad, F., 2003. Protein tyrosine nitration in the mitochondria from diabetic mouse heart. Implications to dysfunctional mitochondria in diabetes. Journal of Biological Chemistry 278:33972–33977.

[64] Boudina, S., Bugger, H., Sena, S., O'Neill, B.T., Zaha, V.G., Ilkun, O., et al., 2009. Contribution of impaired myocardial insulin signaling to mitochondrial dysfunction and oxidative stress in the heart. Circulation 119:1272–1283.

[65] Brand, M.D., Esteves, T.C., 2005. Physiological functions of the mitochondrial uncoupling proteins UCP2 and UCP3. Cell Metabolism 2:85–93.

[66] Bugger, H., Abel, E.D., 2010. Mitochondria in the diabetic heart. Cardiovascular Research 88:229–240.

[67] Maalouf, M., Sullivan, P.G., Davis, L., Kim, D.Y., Rho, J.M., 2007. Ketones inhibit mitochondrial production of reactive oxygen species production following glutamate excitotoxicity by increasing NADH oxidation. Neuroscience 145:256–264.

[68] Maalouf, M., Rho, J.M., 2008. Oxidative impairment of hippocampal long-term potentiation involves activation of protein phosphatase 2A and is prevented by ketone bodies. Journal of Neuroscience Research 86:3322–3330.

 

[69] Holmstrom, K.M., Finkel, T., 2014. Cellular mechanisms and physiological consequences of redox-dependent signalling. Nature Reviews Molecular Cell Biology 15:411—421.

[70] Foster, D.B., Liu, T., Rucker, J., O'Meally, R.N., Devine, L.R., Cole, R.N., et al., 2013. The cardiac acetyl-lysine proteome. PLoS ONE 8:e67513.

[71] Nguyen, T.T., Wong, R., Menazza, S., Sun, J., Chen, Y., Wang, G., et al., 2013. Cyclophilin D modulates mitochondrial acetylome. Circulation Research 113: 1308—1319.

[72] Grillon, J.M., Johnson, K.R., Kotlo, K., Danziger, R.S., 2012. Non-histone lysine acetylated proteins in heart failure. Biochimica Biophysica Acta 1822:607—614.

[73] Sack, M.N., 2012. The role of SIRT3 in mitochondrial homeostasis and cardiac adaptation to hypertrophy and aging. Journal of Molecular and Cellular Cardiology 52:520—525.

[74] Sundaresan, N.R., Gupta, M., Kim, G., Rajamohan, S.B., Isbatan, A., Gupta, M.P., 2009. Sirt3 blocks the cardiac hypertrophic response by augmenting Foxo3a-dependent antioxidant defense mechanisms in mice. Journal of Clinical Investigation 119:2758—2771.

[75] Gupta, M.P., Samant, S.A., Smith, S.H., Shroff, S.G., 2008. HDAC4 and PCAF bind to cardiac sarcomeres and play a role in regulating myofilament contractile activity. Journal of Biological Chemistry 283:10135—10146.

[76] Samant, S.A., Courson, D.S., Sundaresan, N.R., Pillai, V.B., Tan, M., Zhao, Y., et al., 2011. HDAC3-dependent reversible lysine acetylation of cardiac myosin heavy chain isoforms modulates their enzymatic and motor activity. Journal of Biological Chemistry 286:5567—5577.

[77] Shimazu, T., Hirschey, M.D., Newman, J., He, W., Shirakawa, K., Le Moan, N., et al., 2013. Suppression of oxidative stress by beta-hydroxybutyrate, an endogenous histone deacetylase inhibitor. Science 339:211—214.

 